3/5/91 M.L.R. (1)

CONTRACTOR REPORT

SAND90–7019
Unlimited Release
UC–721

Characterization of Fracture Surfaces in Dolomite Rock, Culebra Dolomite Member, Rustler Formation

Terry Sewards
Department of Geology & Institute of Meteoritics
University of New Mexico
Albuquerque, NM 87131

Prepared by Sandia National Laboratories Albuquerque, New Mexico 87185
and Livermore, California 94550 for the United States Department of Energy
under Contract DE-AC04-76DP00789

Printed March 1991

Issued by Sandia National Laboratories, operated for the United States Department of Energy by Sandia Corporation.

Printed in the United States of America. This report has been reproduced directly from the best available copy.

Available to DOE and DOE contractors from
Office of Scientific and Technical Information
PO Box 62
Oak Ridge, TN 37831

Prices available from (615) 576-8401, FTS 626-8401

Available to the public from
National Technical Information Service
US Department of Commerce
5285 Port Royal Rd
Springfield, VA 22161

NTIS price codes
Printed copy: A04
Microfiche copy: A01

SAND90-7019
Unlimited Release
Printed March 1991

Distribution
Category UC-721

CHARACTERIZATION OF FRACTURE SURFACES IN DOLOMITE ROCK, CULEBRA DOLOMITE MEMBER, RUSTLER FORMATION*

Terry Sewards

Department of Geology and Institute of Meteoritics
University of New Mexico, Albuquerque, NM 87131

ABSTRACT

The Culebra Dolomite Member, Rustler Formation, southeastern New Mexico, is characterized by a high fracture porosity. Bedding plane fractures are predominant, but vertical and high-angle fractures are also common. The information presented in this report for horizontal fractures shows that: (1) horizontal water-bearing fractures in dolomite and calcite rock tend to occur in zones where clay and quartz are concentrated, particularly along clay seams, and (2) secondary minerals, primarily gypsum and some calcite, are precipitated from solution onto the fracture surfaces. No surfaces of vertical or high-angle fractures that were clearly identifiable as water-bearing were discovered in the cores examined.

Dolomite compositions on the fracture surfaces are no different than those in the bulk rock, indicating that aqueous alteration of dolomite did not occur to any significant extent. Where present, calcite in these samples, both in the bulk rock and fracture surfaces, is a product of recrystallization from dolomite caused by aqueous alteration, usually near surface.

It is probable that the vertical fracture surfaces are not as clay- rich as the horizontal ones, since accumulations of clay occur along horizontal planes due to sedimentation.

Our data argue that since the cation exchange capacity of clay minerals is so much higher than that of dolomite, calcite, or gypsum, and the clay minerals are a major component of the fracture surface mineralogy, the sorption of radionuclides due to the clay will far outweigh that of the other minerals. This fact should be taken into account in any study of the transport of radionuclides through the Culebra Dolomite.

* The work described in this report was performed for Sandia National Laboratories under Contract No. 01-6328.

DO NOT MICROFILM
THIS PAGE

ACKNOWLEDGMENT

The author wishes to thank John Husler, of the University of New Mexico Geology Department, for the compositional analyses, and Tom Servilla, of the University of New Mexico Institute of Meteoritics, for the thin-section preparation.

The author also acknowledges the contributions made by several scientists from Sandia National Laboratories to this report. S. J. Lambert provided technical guidance for the work, assisted the author in the collection of the samples examined in this study, and provided a critical review of the draft report. M. D. Siegel was the project manager for this work, was responsible for the preparation of the final draft of the report, and coordinated, technical management reviews.

Dr. D. G. Brookins of the University of New Mexico reviewed this report and provided invaluable assistance in preparing materials used in the text, figures, and tables.

CONTENTS

Figures

Figures

Tables

I. INTRODUCTION

The Culebra Dolomite Member of the Rustler Formation in southeastern New Mexico is characterized by a high fracture porosity. Bedding plane fractures are predominant, but vertical and high-angle fractures are also common. In the WIPP-19 drill core (Chapter III), the bedding plane fracture density varies from 3 to 8 per vertical foot below 764 feet depth, and 1 to 3 per vertical foot above 764 feet. Irregularly-curved vertical fractures occur with a frequency of 1 to 4 per vertical foot, and high angle fractures (60 to 70°) are spaced at about 1 to 5 per vertical foot (Ferrall and Gibbons, 1979). Water-bearing (open) fracture surfaces are easily recognized because they are darker than the bulk dolomite due to aqueous alteration.

The objective of this report is to describe the water-bearing fracture surfaces in detail, in terms of texture and mineralogy and to compare and contrast the composition and mineralogy of the surfaces with that of the bulk rocks. Analytical methods used in this study include x-ray diffraction (XRD) analysis, x-ray fluorescence (XRF) spectroscopic analysis, atomic absorption (AA) spectroscopy, electron microscope elemental analysis, and optical microscopy.

II. SITE GEOLOGY

The Upper Permian (Ochoan) Rustler Formation is a sequence of evaporite and clastic rock units deposited in the Delaware, Midland, Palo Duro, and Dalhart Basins in southeastern New Mexico and western Texas. In the Delaware Basin (Figure II-1), which is ringed by the Capitan Reef Complex, the Rustler Formation overlies the Salado Formation, which is composed mainly of thick halite beds and is in turn overlain by the Dewey Lake Red Bed Formation, which is composed almost entirely of mud/siltstone.

The Rustler Formation is divided into four recognizable units (Figure II-2). In ascending order, they are the lower (unnamed) member (argillaceous halite, mud/siltstone, and anhydrite), the Culebra Dolomite Member, the Tamarisk Member (halite, mudstone, anhydrite, and gypsum), the Magenta Dolomite Member, and the Forty-niner Member (anhydrite, gypsum, and mudstone).

In the boreholes from which samples were taken for this study, the Culebra Dolomite Member varies in thickness from about 20 feet to 30 feet. It is primarily composed of massive, laminated dolomite with some clay, quartz, and gypsum, although some cores show extensive brecciation and/or large vugs and voids. Clay laminae of varying thicknesses (2 mm to several centimeters) are common, and the entire unit is underlain by a 0.5 to 3 feet thick black shale (Sewards, Glenn, and Keil, 1991). In the ventilation and access shafts of the WIPP repository, the uppermost 6 to 12" of the black shale are deformed and tilted. This deformation is evidently due to collapse of the dolomite unit. There are no obvious depositional features in the lower 2.5 feet of the black shale. The black shale grades into a reddish/brown shale that is clearly a solution residue: there are no depositional features (laminae, etc.), and the texture is chaotic. This reddish/brown shale overlies the uppermost anhydrite unit in the lower member; the contact is very uneven, but fairly well defined. The anhydrite unit itself is relatively unfractured. It is clear that the dissolution of an argillaceous halite bed above the anhydrite unit and of several other halite units in the lower member and uppermost Salado Formation caused the collapse of the Culebra and overlying units. This collapse resulted in extensive fracturing in the dolomite units (Culebra and Magenta), particularly in the Culebra. The reason that the anhydrite and shale units are not as fractured as the dolomite units is that anhydrite and shale are able to deform in a more plastic manner than the harder dolomite.

In the areas where the dolomite unit lies near the surface, calcite is often present instead of dolomite. This calcite is the result of dedolomitization of dolomite.

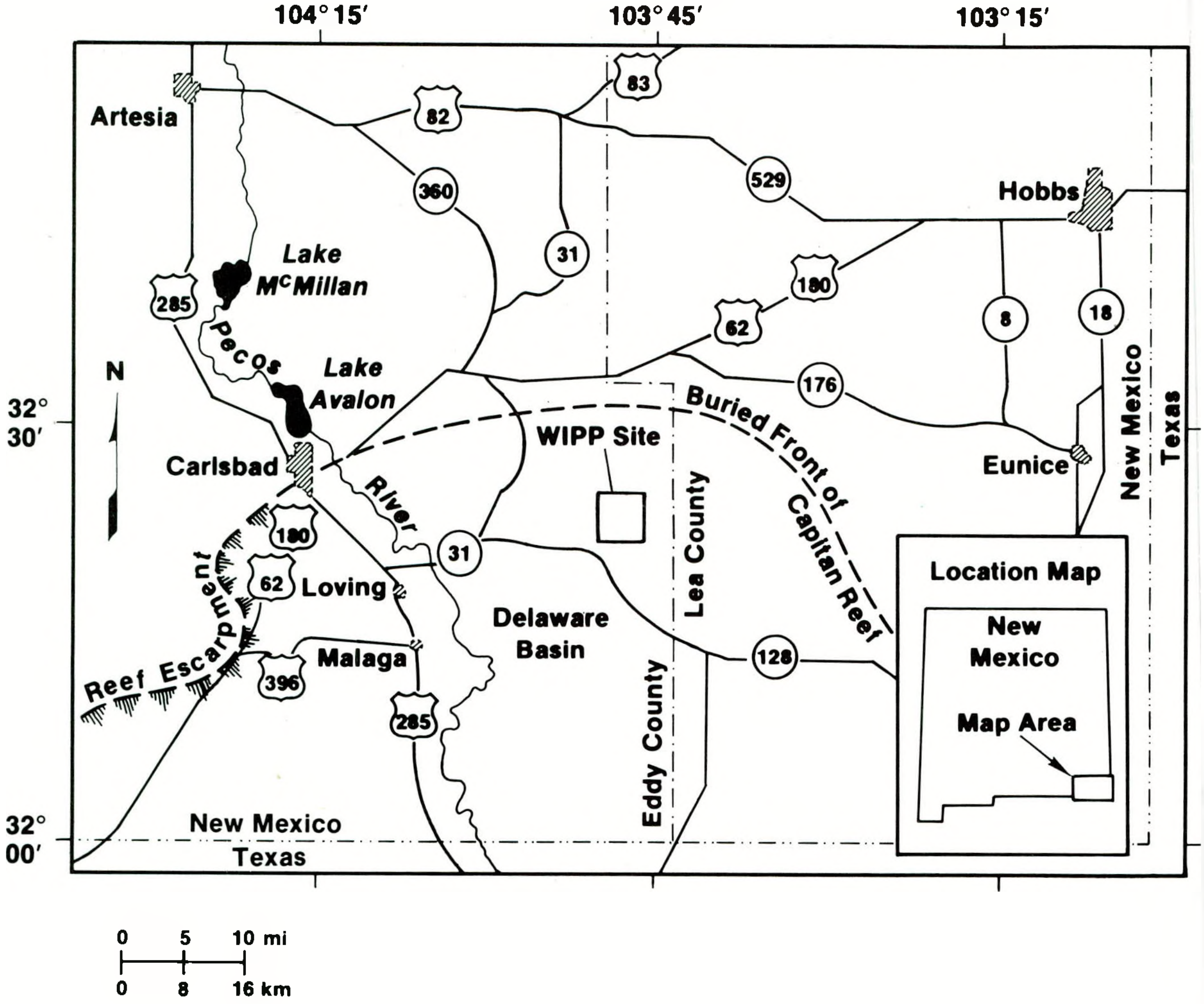

Figure II-1. Regional Setting, Delaware Basin, Southeastern New Mexico (from Borns et al., 1983).

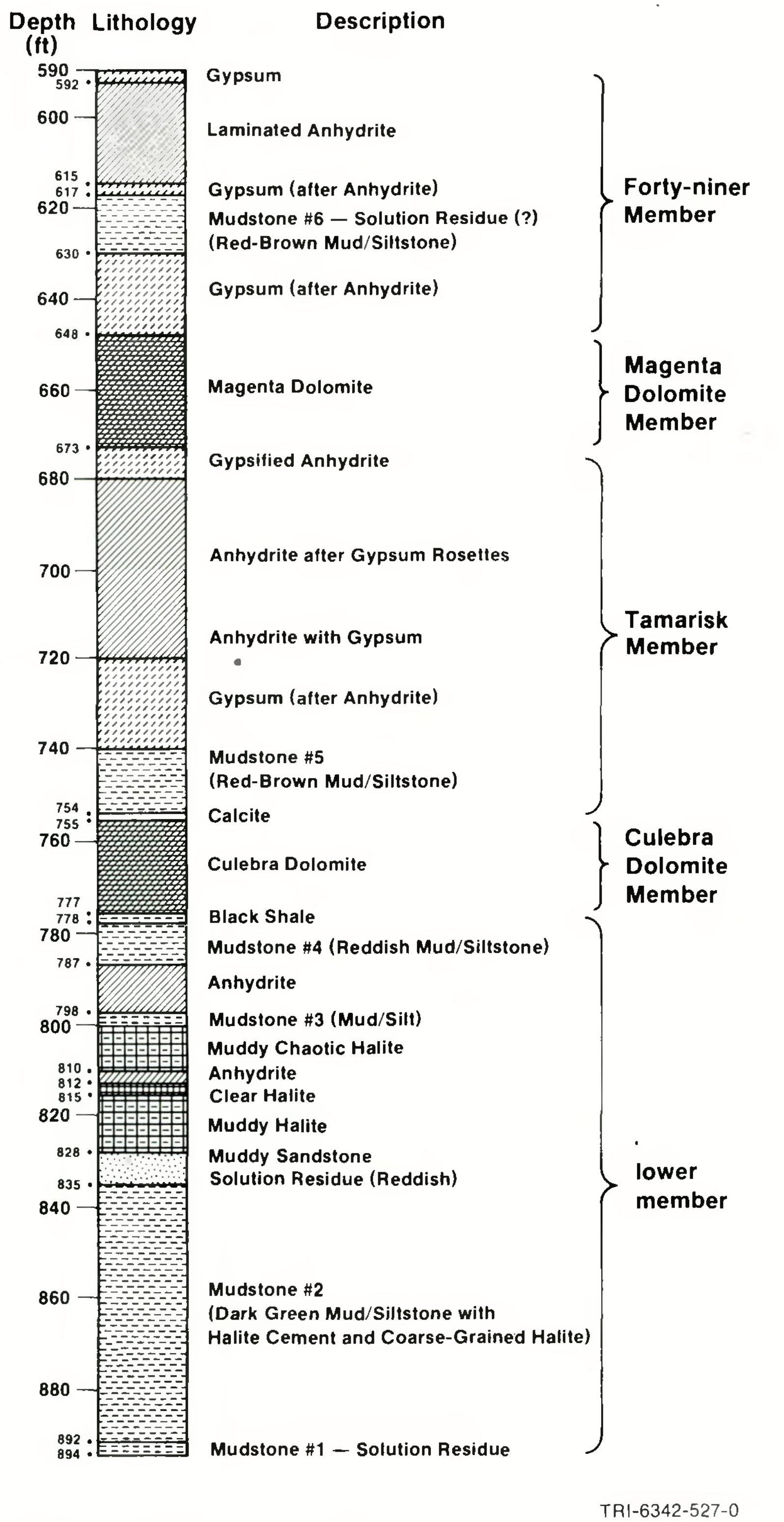

Figure II-2. Lithologic Log of WIPP-19 Core, Rustler Formation (modified from Ferrall and Gibbons, 1979).

III. PROJECT SAMPLES

Eighteen samples were selected from various drill cores located in the vicinity of the Waste Isolation Pilot Plant (WIPP) site (Figure III-1).

Selection Criteria

Samples for this study were selected primarily on the basis of a well-defined, water-bearing fracture surface. Five samples were selected from the WIPP-29 and WIPP-32 cores located in the vicinity of Nash Draw (Figure III-1). In these cores, the Culebra Dolomite is very shallow, and the extra samples were chosen to better characterize the fractures where near surface alteration has occurred.

Core Locations, Sample Depths, and Descriptions

Table III-1 lists the well number, sample depths, and descriptions for the 18 samples selected for this study. Figure III-1 shows the locations of the various wells.

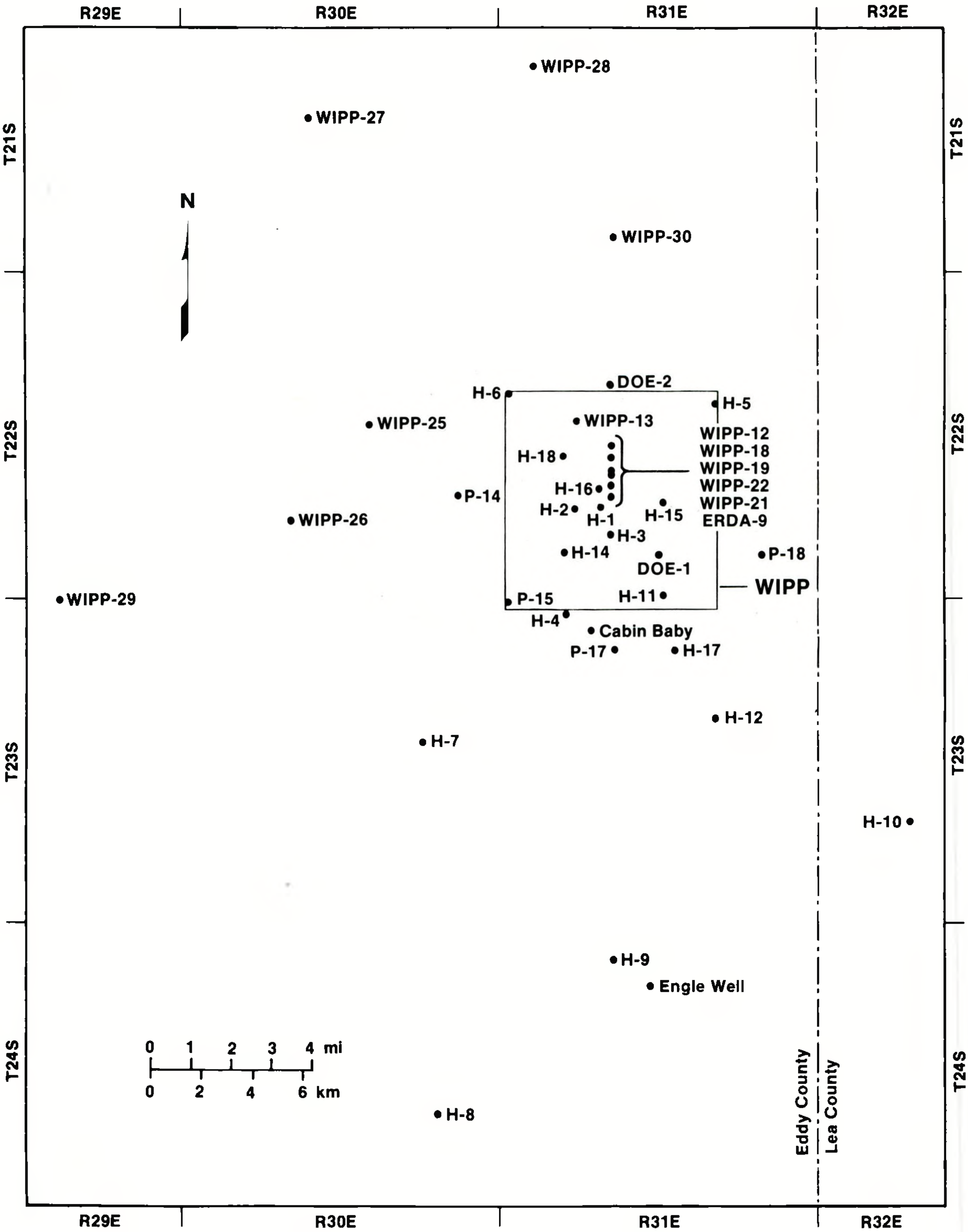

TRI-6342-19-1

Figure III-1. Location of Wells in the Vicinity of the WIPP Site.

Table III-1. Sample Locations and Descriptions

Sample ID	Well	Depth (feet)	Description
CS1	WIPP-12	838.5-838.7	Massive dolomite (vuggy, dark grey)
CS2	WIPP-13	712.1-712.4	Brecciated dolomite (fractured, dark grey)
CS3	WIPP-13	705.3	Massive dolomite (laminated, brown)
CS4	WIPP-13	714.0	Massive dolomite (light brown)
CS5	WIPP-26	187.0	Brecciated dolomite
CS6	WIPP-27	305.0	Brecciated dolomite (friable, light grey)
CS7	WIPP-28	447.5	Massive clay/dolomite (laminated, dark grey)
CS8	WIPP-29	27.0	Massive dolomite (light grey)
CS9	WIPP-30	633.5	Massive dolomite (contorted laminae, tan)
CS10	WIPP-30	639.0	Massive dolomite (vuggy, tan)
CS11	WIPP-30	635.0	Massive dolomite (brecciated, tan)
CS12	WIPP-32	57.0	Massive dolomite (vuggy)
CS13	WIPP-32	91.1	Claystone (grey)
CS14	WIPP-32	55.0	Massive limestone (brown)
CS15	WIPP-32	56.0	Massive limestone (red)
CS16	WIPP-32	62.0	Massive dolomite (light grey)
CS17	WIPP-33	57.0	Massive gypsum (brown)
CS18	WIPP-34	836.0	Massive dolomite (grey)

IV. FRACTURE SURFACE PETROGRAPHY

Hand Specimen Description

Water-bearing fracture surfaces are easily identified in hand specimen: they are much darker (dark grey/brown to black) than freshly broken surfaces (Figures IV-1 to IV-4). The horizontal fractures almost always occur along clay-rich seams, either layers of nearly pure clay or dolomite (and calcite) layers that are especially rich in clay minerals (Figures IV-1 and IV-4). The darkening can be attributed to two factors: (1) the presence of clay minerals (clay separates from Culebra Dolomite rocks are usually dark grey to black), and (2) oxidation of surface minerals due to contact with oxygen-rich waters. The zone of penetration of the darkened (altered) surface area is usually not deep, typically a few tens of microns, but in some samples where the rock near the fracture surface is friable, the darkened zone can penetrate a few millimeters. When the fracture occurs along a layer of pure clay, a dense system of horizontal fractures may develop, rather than a single fracture. Clay layers may be stripped away to reveal successive darkened (altered) surfaces, which are only a few tens or hundreds of microns apart. Thus, a clay seam can become a multilayer channel and present a very large surface area to the fluid moving in the fractures. Fractures that occur in rock that is primarily dolomite or calcite are single layered, and the altered zone is shallow.

Figure IV-3 shows a very pitted fracture surface. This surface is similar to the interior of large vugs that are frequently seen in Culebra Dolomite. Although the majority of the vugs are not interconnected and do not form a part of the transport network, some undoubtedly do, and this surface may be part of a large void in which water did flow.

Optical Microscopy

Polished thin sections perpendicular to the fracture surfaces were prepared from samples in which the surface was not too friable. Of the eight sections prepared, only four fracture surface rims were preserved: CS1, CS4, CS14, and CS18 (Figures IV-6 to IV-9).

Figure IV-5 shows a clay-rich area along the fracture surface rim. The clay area dominates the rim, and very little dolomite is directly on the surface. Areas like this one are not unusual, but the zone near the fracture rim shown in Figure IV-6 is a far more common feature. This area is quite clay-rich, but the rim itself appears to be composed of about 50% clay and 50% dolomite.

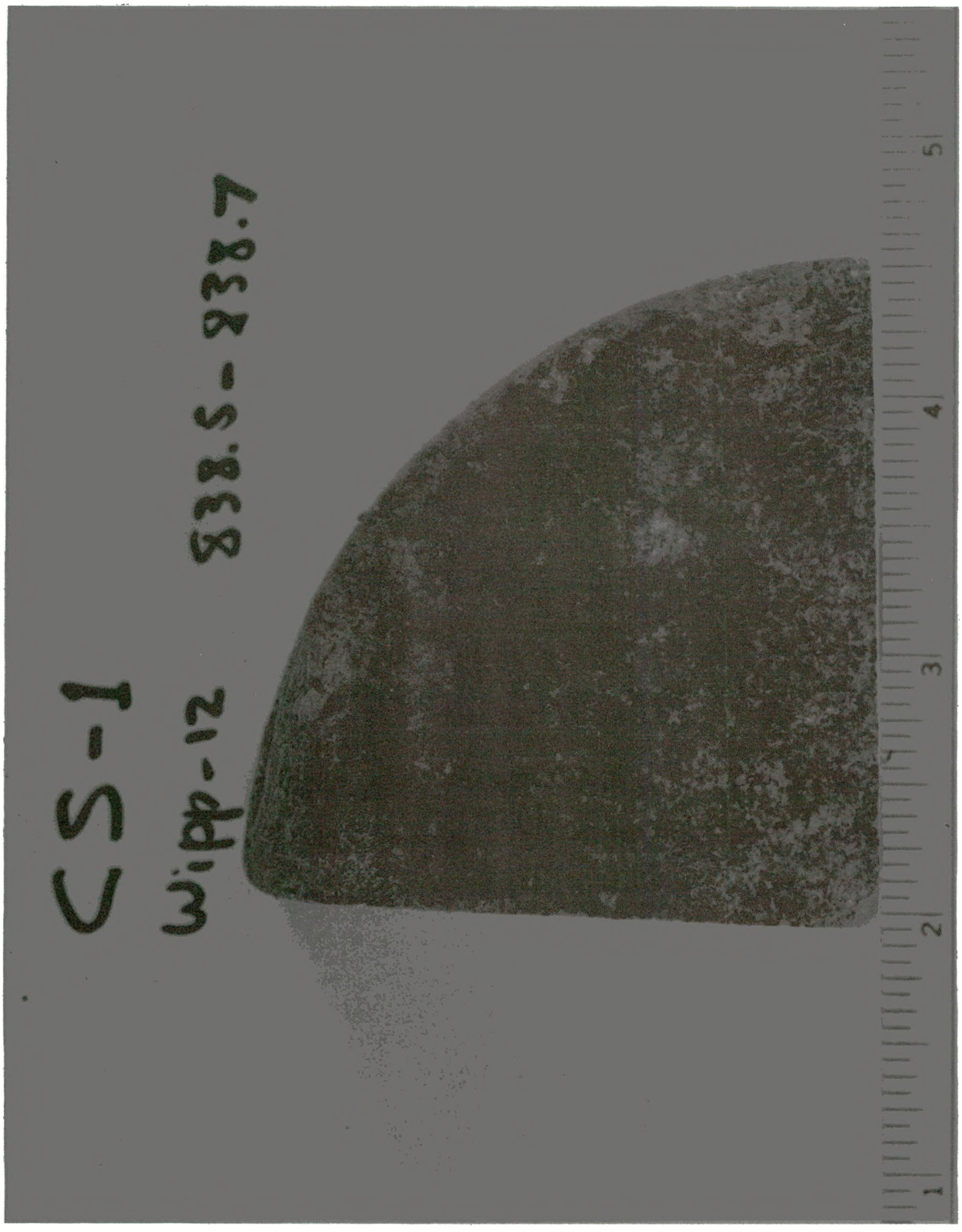

Figure IV-1. Fracture Surface of Sample CS1, Top View.

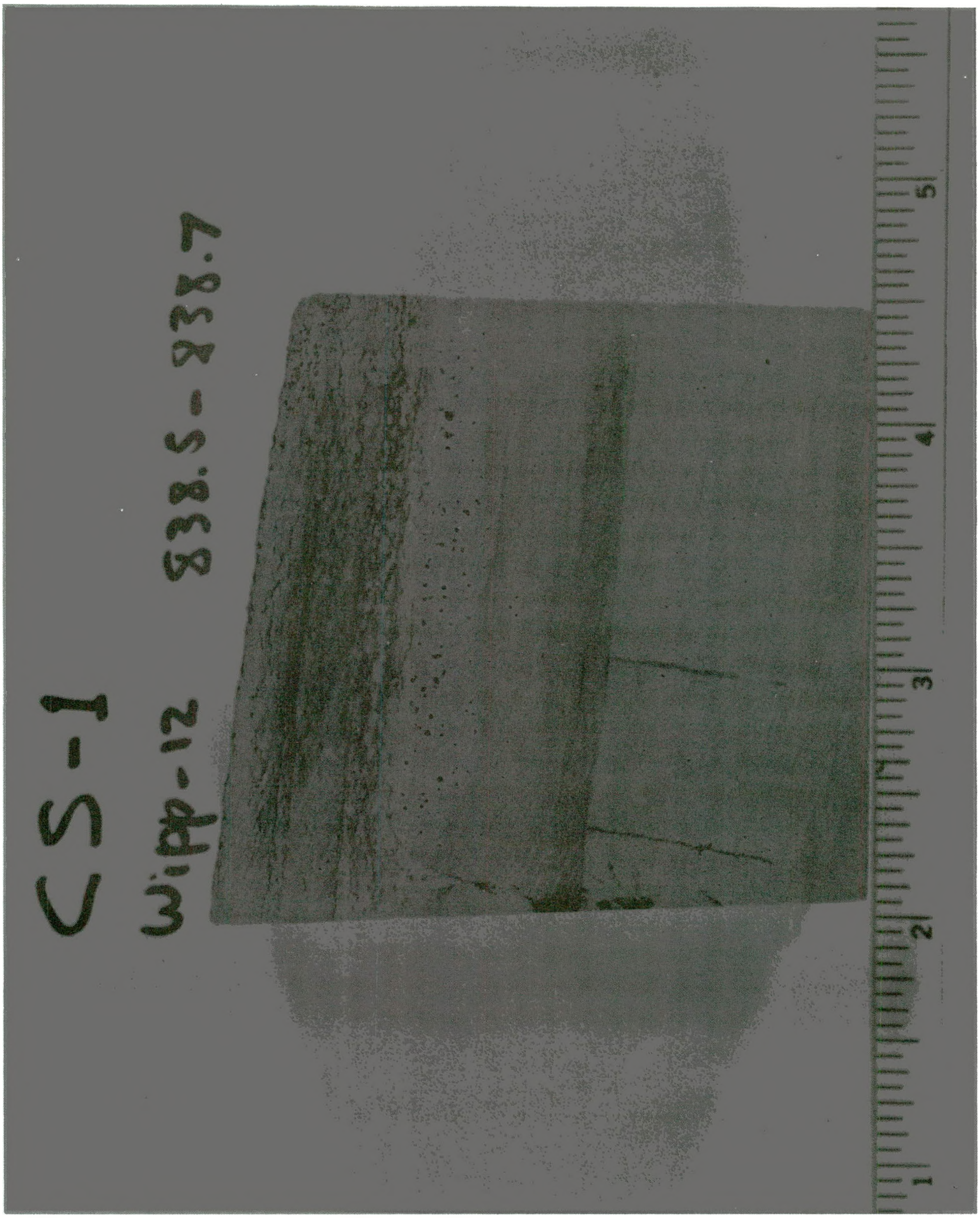

Figure IV-2. Fracture Surface of Sample CS1, Side View.

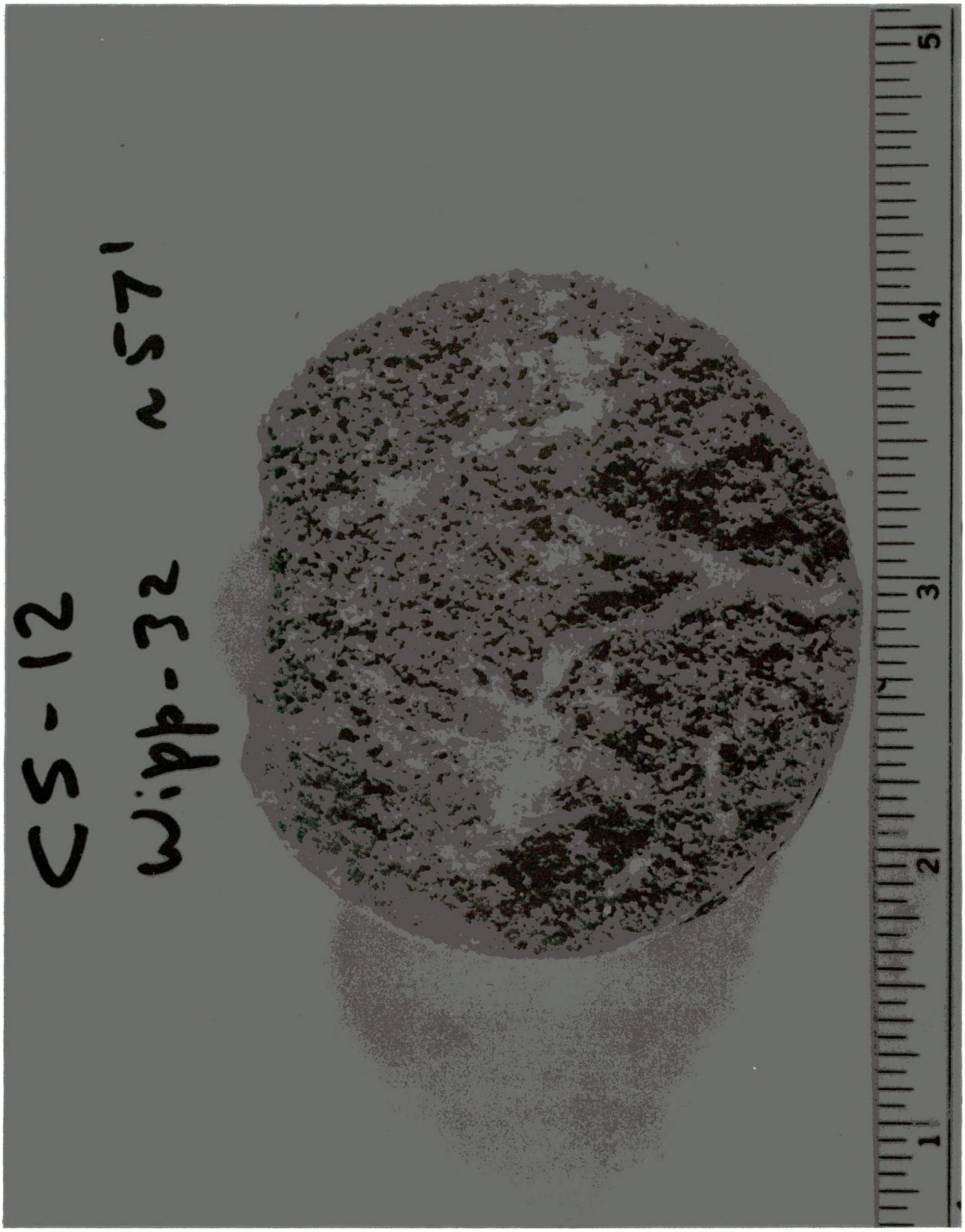

Figure IV-3. Fracture Surface of Sample CS12, Top View.

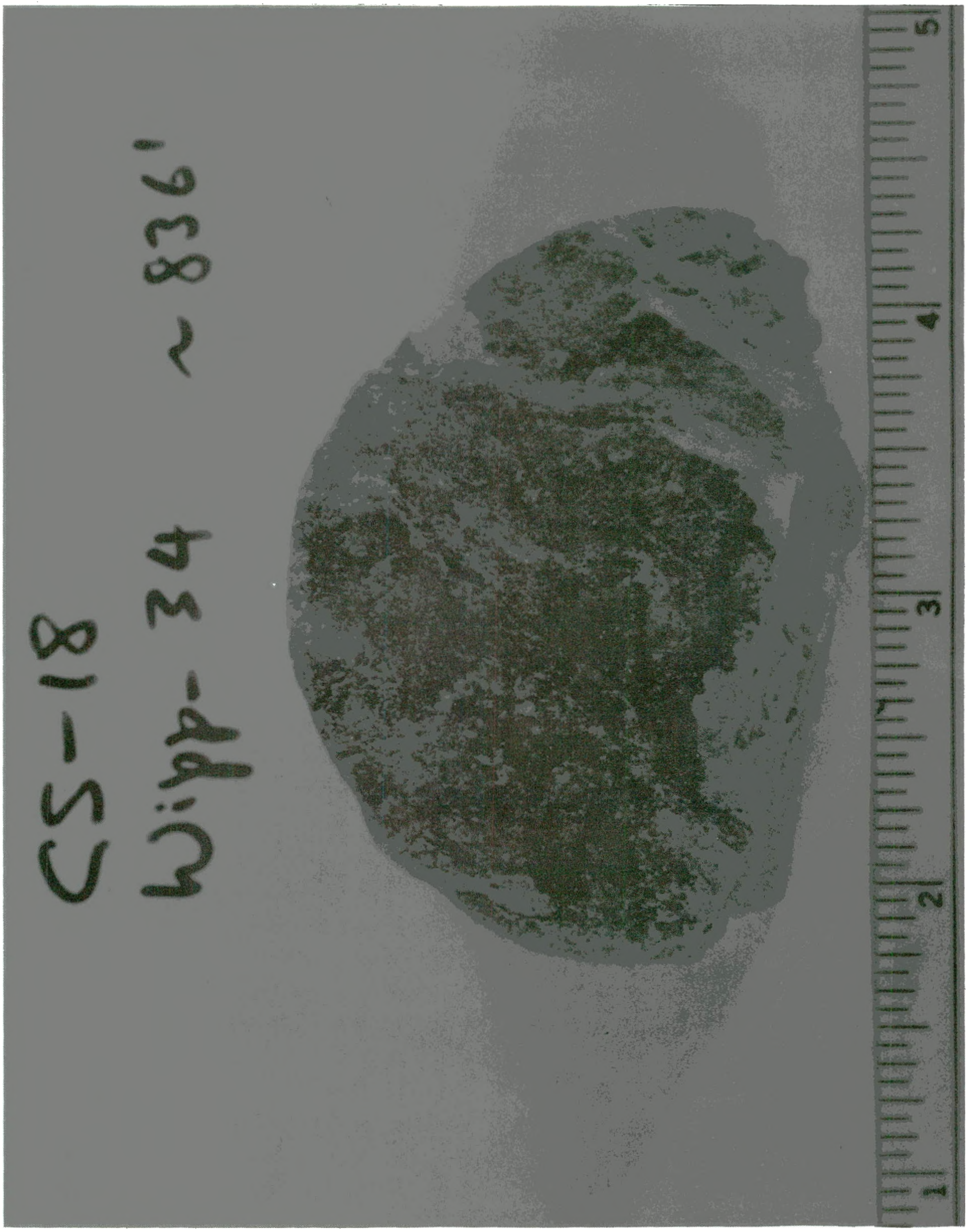

Figure IV-4. Fracture Surface of Sample CS18, Top View.

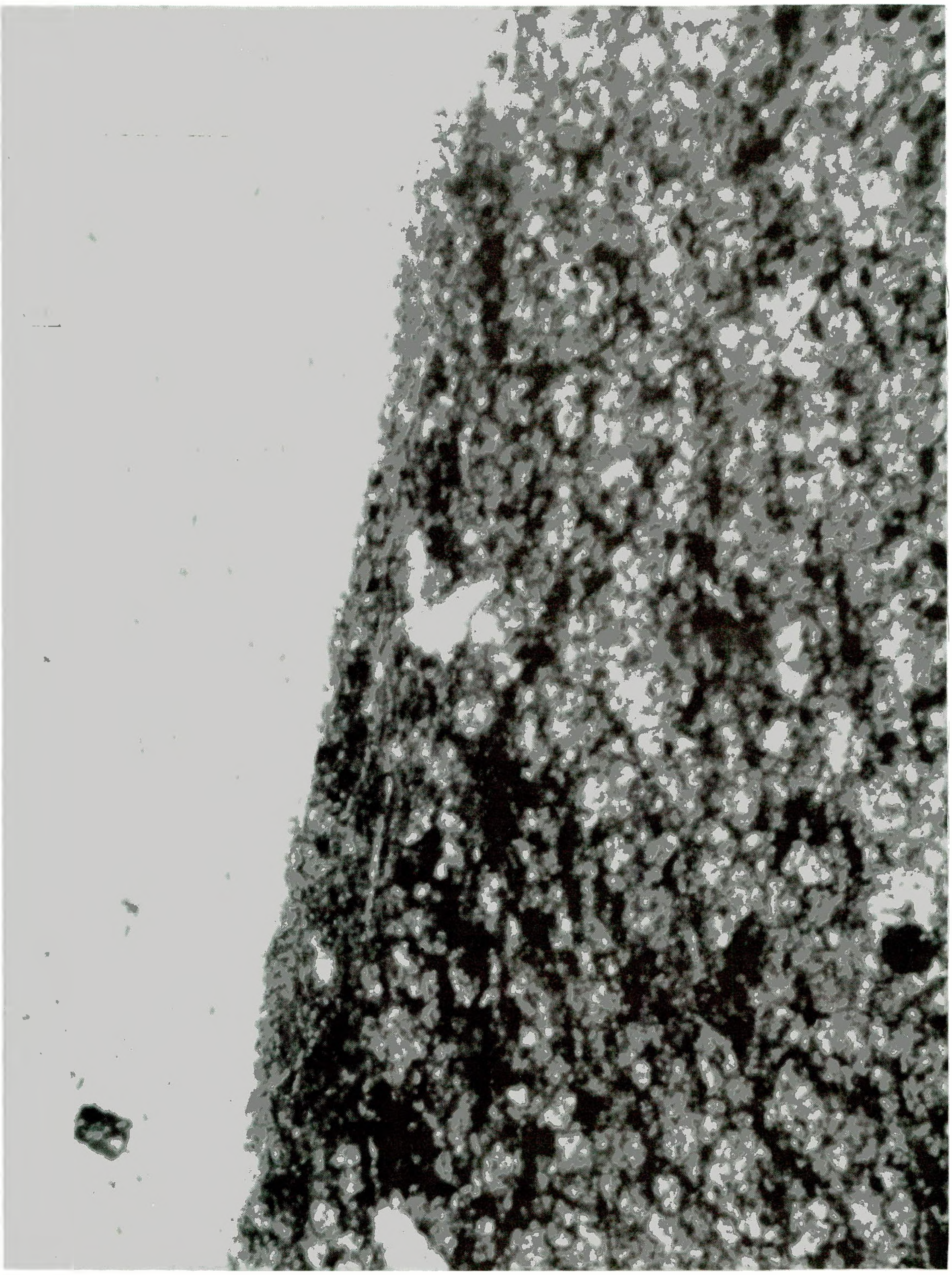

Figure IV-5. Thin-Section Photomicrograph of Fracture Surface Rim of Sample CS4. Plane polarized light, M = 1000X. Note dense clay-rich area on surface rim.

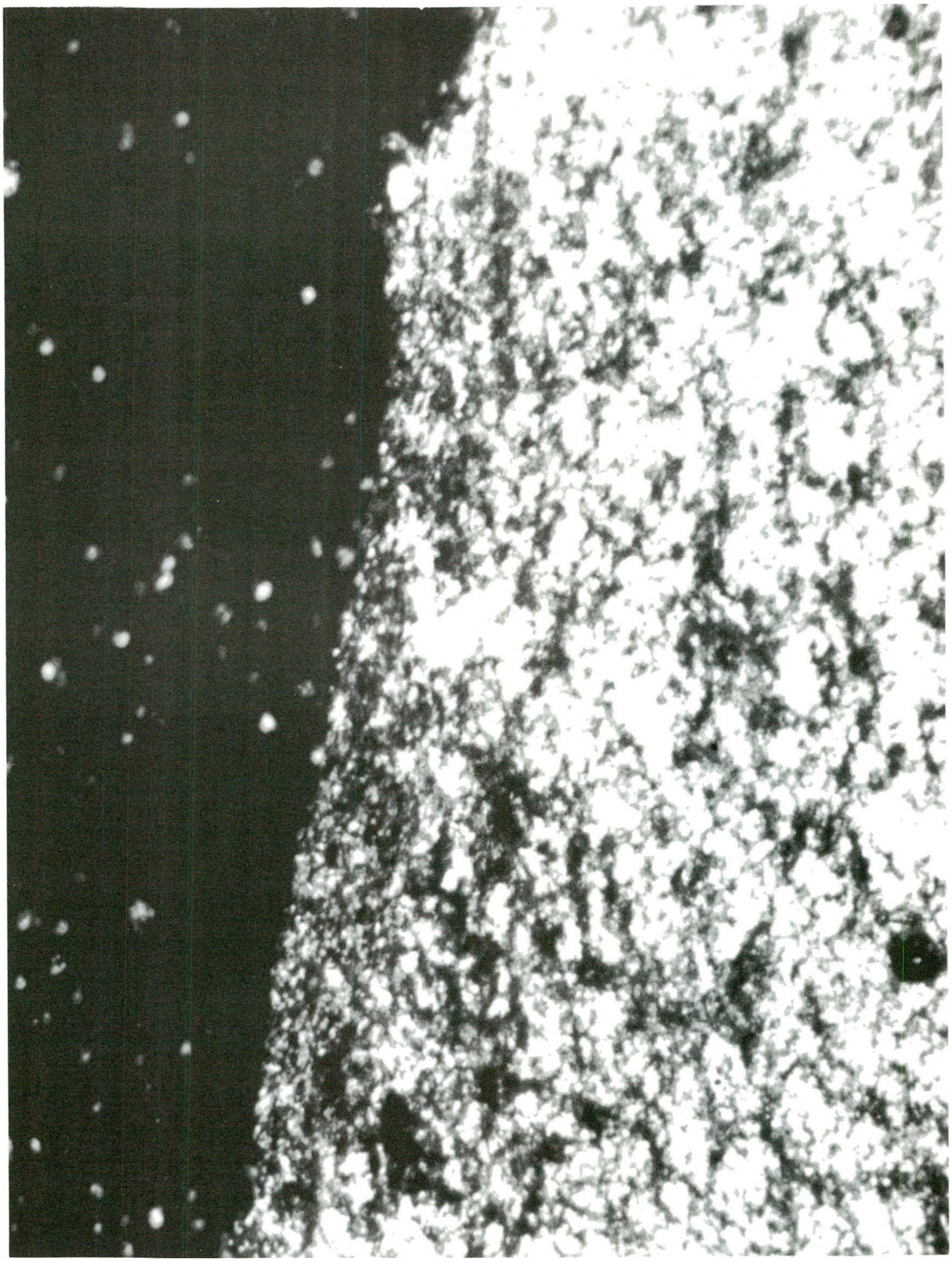

Figure IV-6. Thin-Section Photomicrograph of Fracture Surface Rim of Sample CS4. Crossed polars, M=1000X. Note clay-rich area near surface rim.

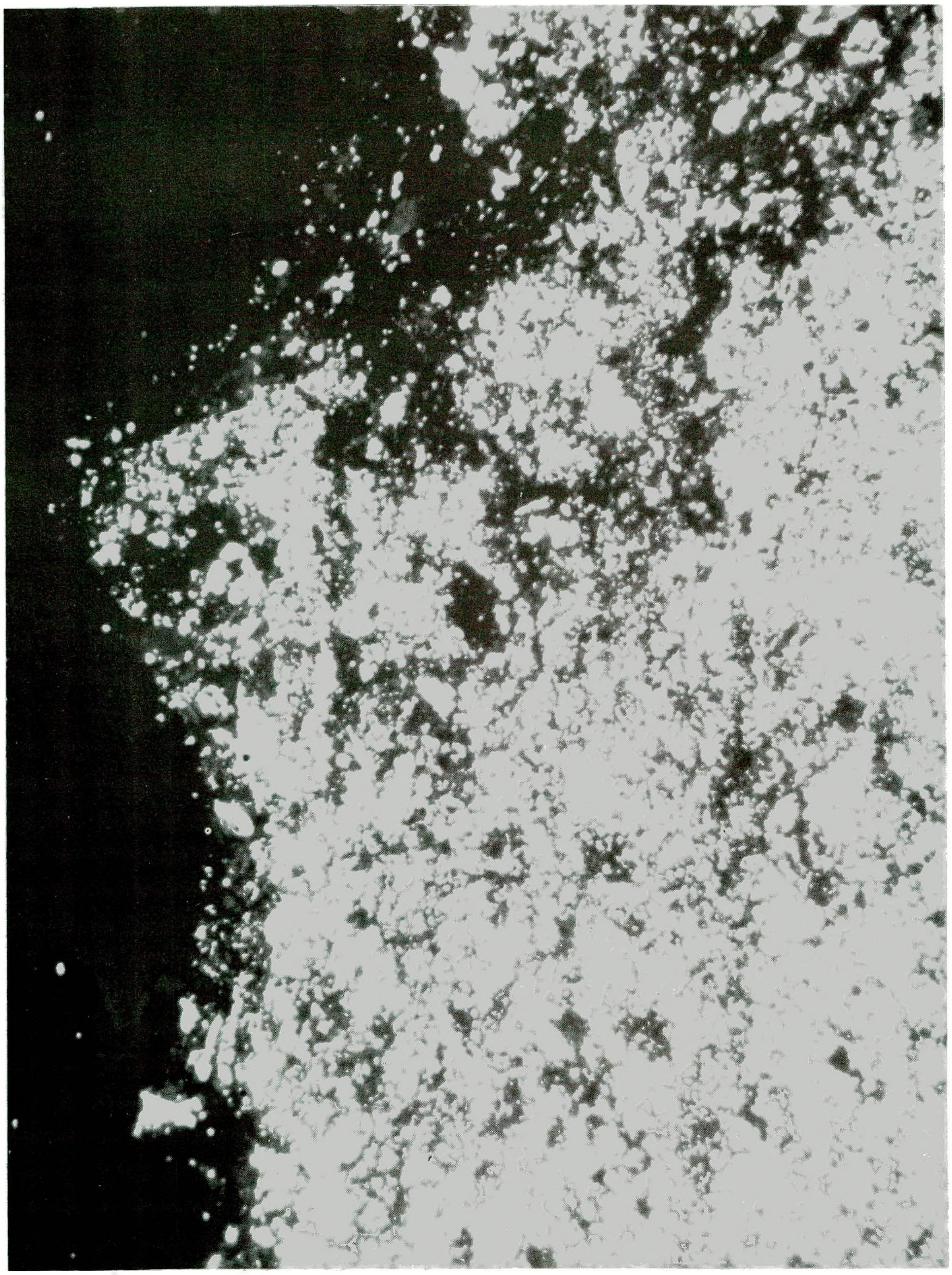

Figure IV-7. Thin-Section Photomicrograph of Fracture Surface Rim of Sample CS4. Crossed polars, M=1000X. Note gypsum lining on fracture rim.

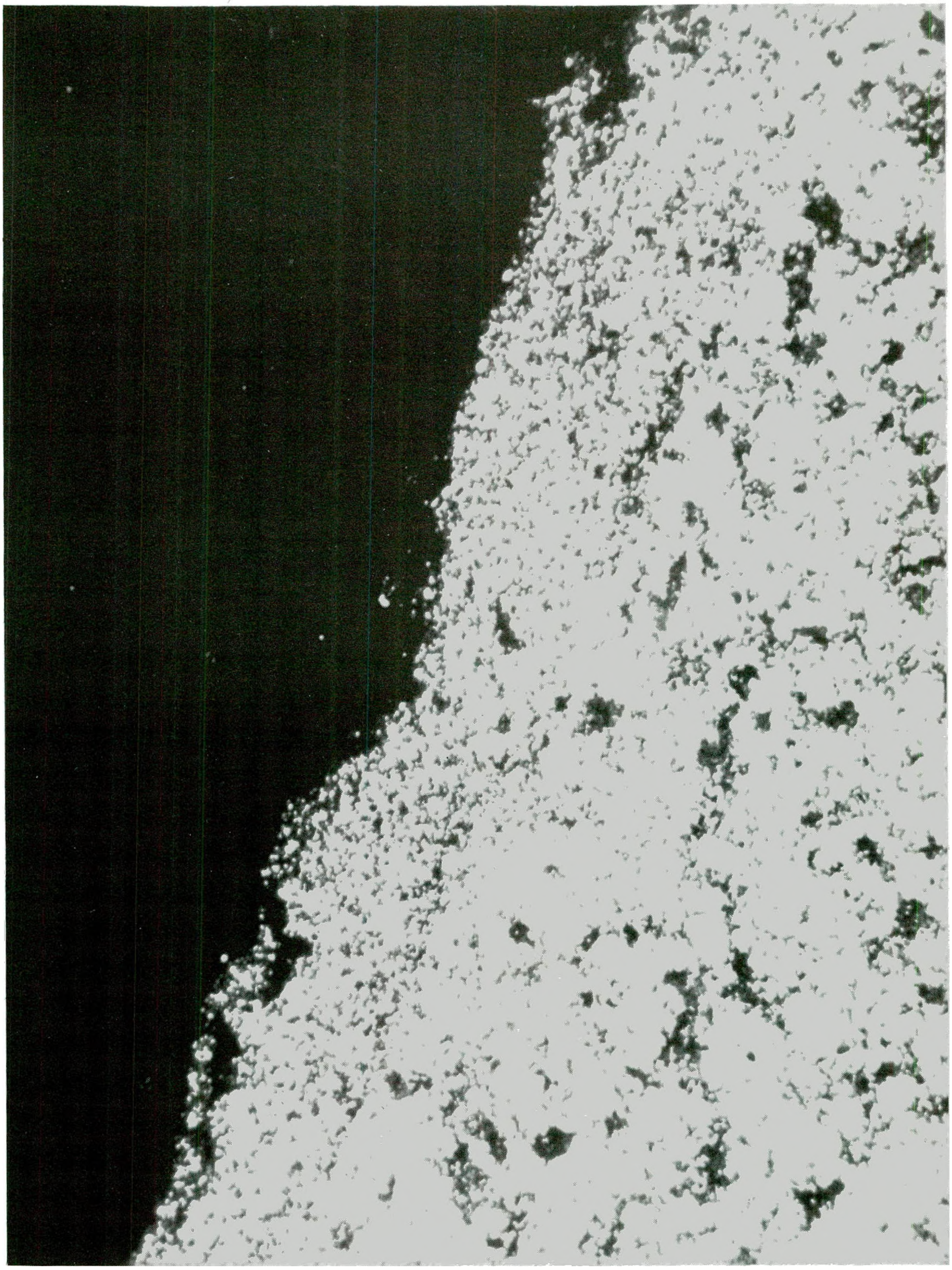

Figure IV-8. Thin-Section Photomicrograph of Fracture Surface Rim of Sample CS18. Crossed polars, M = 1000X. Note fine-grained dolomite on fracture rim.

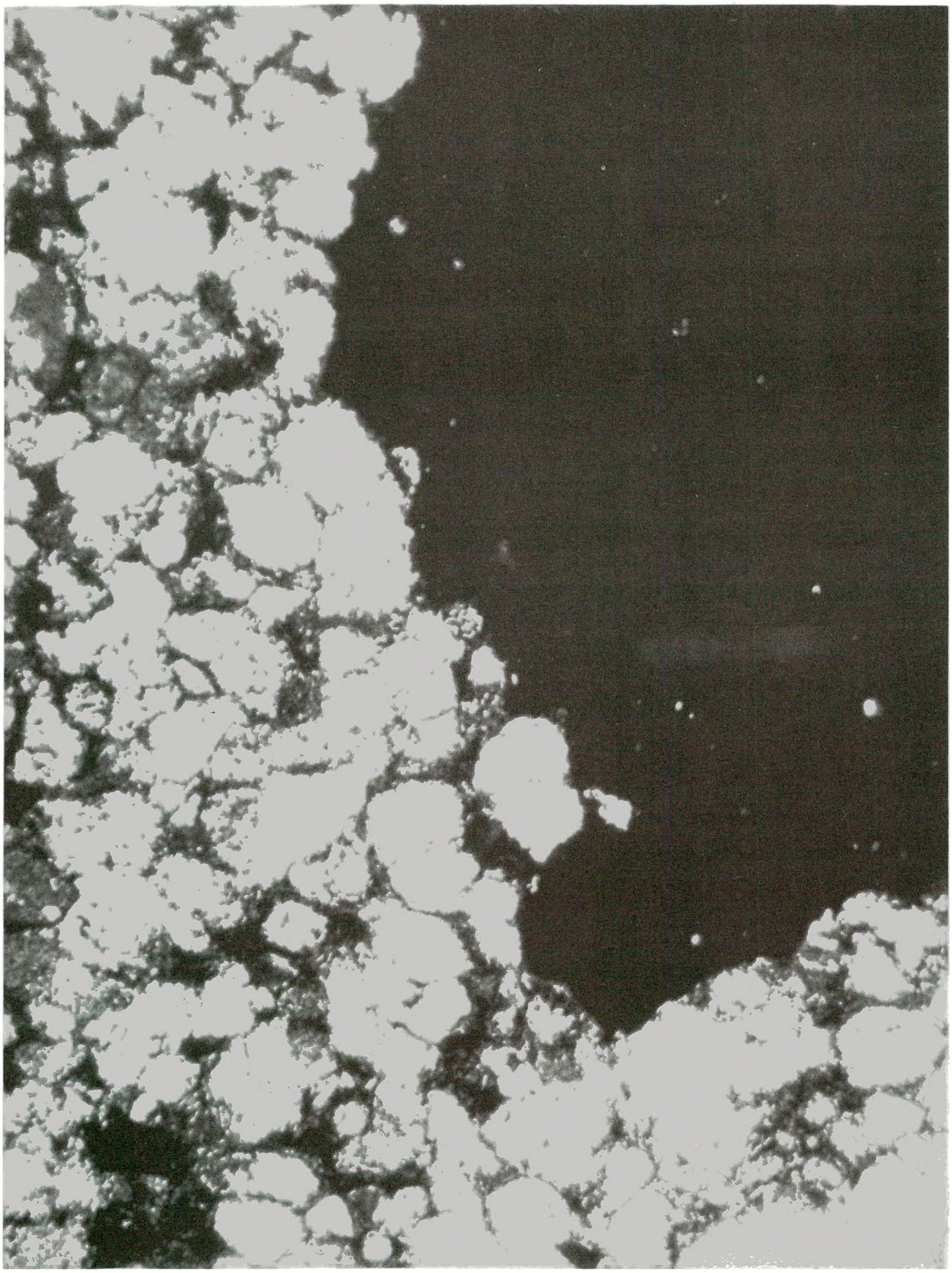

Figure IV-9. Thin-Section of Photomicrograph of Fracture Surface Rim of Sample CS15. Crossed polars, M = 1000X.

Figure IV-7 shows a gypsum and clay-rich area near the fracture surface. Along the rim, a lining of gypsum shields the clay from the fracture surface, so there was probably little contact between the water moving in the fracture and the clay minerals near the surface.

In Figure IV-8 there is an area of extremely fine-grained dolomite near the fracture surface. This area appears to be free of clay. The average grain size in the normal dolomite away from the rim is about 7μm, compared to about 0.6μm in the fine-grained area. This feature was not observed in the other thin sections or elsewhere in the thin section of sample CS4 and is probably fairly rare. It may be interpreted in one of two ways: (1) the fine-grained area is a zone of alteration in which the dolomite has recrystallized into "micromicritic" dolomite, or (2) the area is a primary feature, and the fracture traversed the fine-grained area because the rock was weaker there. Neither explanation is particularly satisfactory since, in the first case, dolomite that recrystallizes from calcite, for example, is invariably coarse-grained; in the second case, it would be a great coincidence for such an unusual feature to be directly in the path of the fracture.

Figure IV-9 shows coarse-grained calcite (about 25μm in diameter) near the fracture rim of sample CS15, a limestone. Although the area is clay-rich, calcite grains dominate the fracture rim itself. The texture and grain size of the calcite are typical for the limestones, both near the fracture surfaces and away from them, although larger grain sizes were observed, and twinned crystals are common. This coarse-grained subhedral calcite is quite different from that found at the top of the Culebra in the WIPP-19 core (754' depth, Sewards, Glenn, and Keil, 1991). In that case, the calcite was micritic (grain size about 4-5μm), with anhedral grains, and very clay-rich. The difference in texture might be explained by assuming that the calcite in the WIPP-19 core is the result of primary deposition, and the coarse-grained calcite observed in these samples is the result of dedolomitization (calcitization) of dolomite due to near surface aqueous alteration.

V. WHOLE ROCK AND FRACTURE SURFACE COMPOSITIONS

The compositional data for the bulk rock and fracture surfaces, measured in component oxides, are listed in Tables V-1 and V-2. These tables are derived from Tables C-1 and C-2 in Appendix C by subtracting the halite component and renormalizing. The data for the bulk rock were obtained by x-ray fluorescence spectroscopic analysis (XRF), with the exception of the values for SO_3, which were measured gravimetrically. For the fracture surface analyses, atomic absorption spectroscopy (AA) was used, with the exception of the sulfate measurements. Based on the totals, it is estimated that the XRF data for the bulk rock are accurate to about 10% of the amounts present. The fracture surface analyses were obtained from scrapings from the surfaces, and very little material was obtained (typically 50 mg). The AA data for such a small sample are probably not accurate to more than about 50% of the amount present.

Figures V-1 to V-8 show the composite bulk rock and fracture surface abundances of SiO_2, Al_2O_3, MgO, and CaO in bar-diagram form. In the bar-diagrams, it can be easily seen that SiO_2 is greatly concentrated on the fracture surfaces (Figures V-1 and V-2). In all samples, except CS7 and CS13, the fracture surface concentration is greater than the bulk rock concentration (in samples CS1 and CS3 the fracture surface concentrations were not measured due to insufficient sample). Similarly, Al_2O_3 is higher in concentration on the fracture surfaces in all samples (Figures V-3 and V-4), with the same two exceptions mentioned above, CS7 and CS13. The increase in SiO_2 and Al_2O_3 can be explained by the fact that fracture surfaces tend to occur along clay- and quartz-rich seams in the rock.

The fracture surface MgO concentrations are lower than those in the bulk rock in all samples except CS6, CS12, CS14, CS15, and CS17 (Figures V-5 and V-6). since MgO occurs in both clay and dolomite, its behavior is not quite as easily explained as that of SiO_2 and Al_2O_3, which occur only in the clastic components. An increase in clay and quartz on the fracture surfaces is accompanied by a decrease in dolomite, so if the sample contains primarily dolomite (as in samples CS1 to CS11), one would expect a slight decrease in MgO if both SiO_2 and Al_2O_3 increase. The increase in MgO on the fracture surfaces of samples CS14, CS15, and CS17 is due to the fact that CS14 and CS15 are limestones and contain primarily calcite, and CS17 is gypsum: since the fractures occur along clay-rich seams, and there is essentially no MgO in the major mineral components, MgO is consequently enriched on the surfaces.

The behavior of CaO is also somewhat complicated, since it is a component of dolomite, calcite, and gypsum. In dolomite rocks (CS1 through CS12, CS16 and CS18), one would expect CaO to be higher in the bulk rock than in the fracture

Table V-1. Bulk Rock Compositions

Sample ID	Well	Depth	SiO_2	TiO_2	Al_2O_3	Fe_2O_3	MnO	MgO	CaO	Na_2O	K_2O	P_2O_5	SO_3	Total
CS1B	WIPP-12	838.60	1.27	0.02	0.24	0.34	0.03	20.22	29.50	0.07	0.07	0.04	0.16	51.94
CS2B	WIPP-13	712.30	4.87	0.08	1.15	0.60	0.02	19.50	27.40	0.04	0.37	0.04	0.07	54.13
CS3B	WIPP-13	705.30	4.14	0.06	0.98	0.47	0.03	19.27	27.80	0.06	0.31	0.04	0.07	53.23
CS4B	WIPP-13	714.00	5.56	0.05	1.14	0.56	0.02	19.30	27.60	0.05	0.37	0.04	0.04	54.72
CS5B	WIPP-26	187.50	2.82	0.04	0.65	0.37	0.04	19.65	27.80	0.07	0.29	0.04	0.05	51.81
CS6B	WIPP-27	305.00	1.95	0.03	0.41	0.29	0.02	20.05	27.90	0.25	0.24	0.05	0.09	51.28
CS7B	WIPP-28	447.50	24.02	0.29	5.51	0.78	0.03	19.02	18.89	1.29	1.19	0.03	0.10	71.15
CS8B	WIPP-29	27.00	3.73	0.06	0.84	0.44	0.02	19.80	27.50	0.22	0.34	0.05	0.06	53.05
CS9B	WIPP-30	633.50	14.27	0.17	2.81	0.09	0.01	19.15	26.14	1.75	1.12	0.13	0.19	65.83
CS10B	WIPP-30	639.00	2.70	0.04	0.55	0.34	0.02	20.40	29.90	0.05	0.18	0.10	0.05	54.32
CS11B	WIPP-30	635.00	1.35	0.02	0.33	0.30	0.02	20.05	29.80	0.30	0.13	0.10	0.07	52.46
CS12B	WIPP-32	57.00	0.35	0.01	0.10	0.08	0.01	11.40	43.60	0.05	0.02	0.18	0.12	55.92
CS13B	WIPP-32	91.10	53.36	0.74	12.96	4.32	0.01	16.15	0.95	0.05	2.32	0.21	0.03	91.10
CS14B	WIPP-32	55.00	2.20	0.02	0.38	0.15	0.02	0.84	54.40	0.04	0.13	0.25	0.13	58.56
CS15B	WIPP-32	56.00	2.95	0.03	0.50	0.22	0.02	0.84	52.60	0.04	0.17	0.25	0.12	57.73
CS16B	WIPP-32	62.00	1.55	0.02	0.32	0.14	0.01	17.40	32.50	0.05	0.12	0.12	0.07	52.30
CS17B	WIPP-33	570.00	1.77	0.02	0.24	0.10	0.00	0.35	32.20	0.10	0.04	N.A.	45.97	80.79
CS18B	WIPP-34	836.00	2.45	0.04	0.50	0.34	0.02	20.20	27.80	0.06	0.18	0.10	0.09	51.77

Table V-2. Fracture Surface Compositions (NaCl Data Subtracted)

Sample ID	Depth	SiO_2	Al_2O_3	Fe_2O_3	MgO	CaO	K_2O	SO_3	Total
CS1S	838.60	*	7.80	1.11	15.61	35.67	0.89	*	61.09
CS2S	712.30	16.42	4.54	1.32	17.64	21.27	1.23	*	62.43
CS3S	705.30	*	2.69	0.72	17.97	24.07	1.05	*	46.49
CS4S	714.00	17.28	4.61	1.66	18.28	20.38	0.13	1.48	63.83
CS5S	187.50	10.50	1.43	0.48	19.03	26.31	0.62	*	58.38
CS6S	305.00	3.74	0.65	0.28	20.41	28.51	0.32	*	53.09
CS7S	447.50	20.07	4.95	1.36	18.54	19.75	0.93	0.03	65.62
CS8S	27.00	11.16	1.82	1.48	10.19	24.53	1.25	*	50.43
CS9S	633.50	24.82	6.13	1.66	16.27	16.40	1.95	*	67.24
CS10S	639.00	39.37	8.12	2.06	11.83	10.55	2.16	*	74.10
CS11S	635.00	7.27	2.11	0.58	17.46	26.88	0.61	3.37	58.28
CS12S	57.00	0.98	0.14	0.12	13.26	40.57	0.06	*	55.13
CS13S	91.10	45.79	11.13	3.14	11.37	11.23	1.57	0.29	84.53
CS14S	55.00	28.92	6.88	2.10	9.82	24.04	1.83	0.01	73.60
CS15S	56.00	25.74	5.98	1.97	8.01	28.78	1.34	0.01	71.82
CS16S	62.00	4.56	0.71	0.33	16.91	34.03	0.24	0.61	57.40
CS17S	57.00	28.69	5.82	2.15	4.70	17.64	1.31	21.09	81.40
CS18S	836.00	9.91	2.55	4.21	16.37	28.69	0.66	*	62.40

* ≈ Insufficient Sample

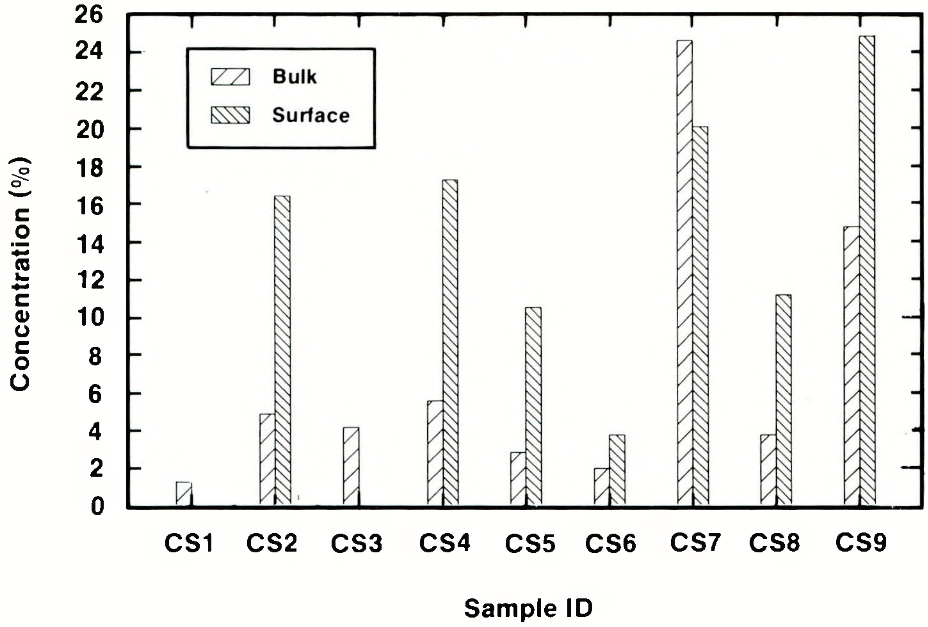

TRI-6342-453-0

Figure V-1. SiO_2 Concentrations of CS1 through CS9.

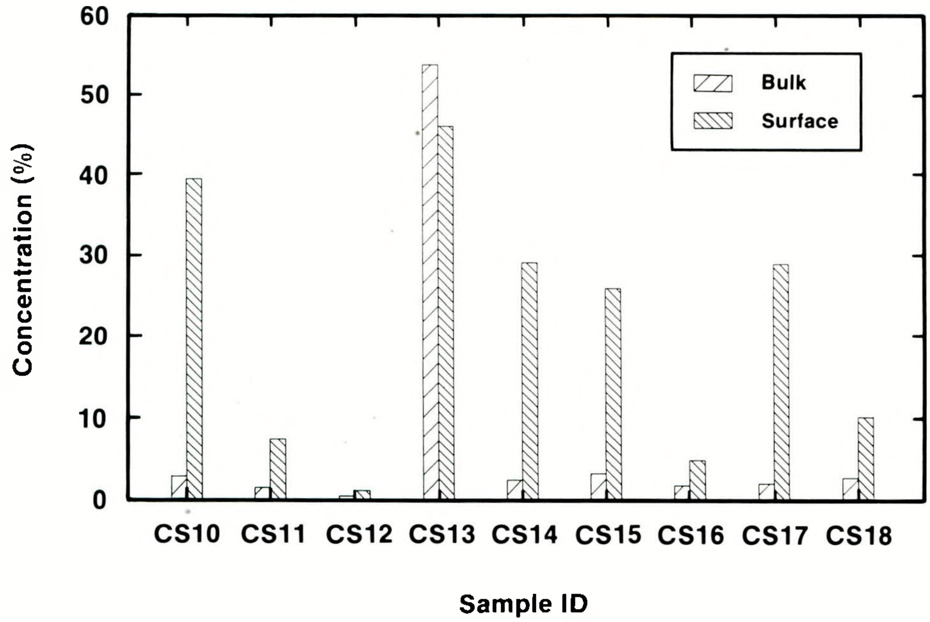

TRI-6342-454-0

Figure V-2. SiO_2 Concentrations of CS10 through CS18.

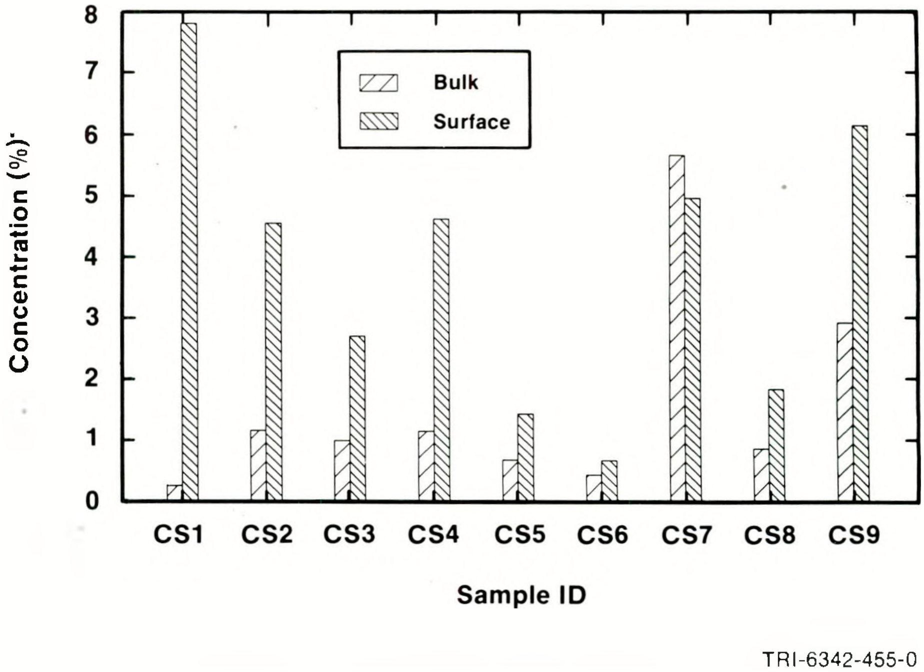

Figure V-3. Al_2O_3 Concentrations of CS1 through CS9.

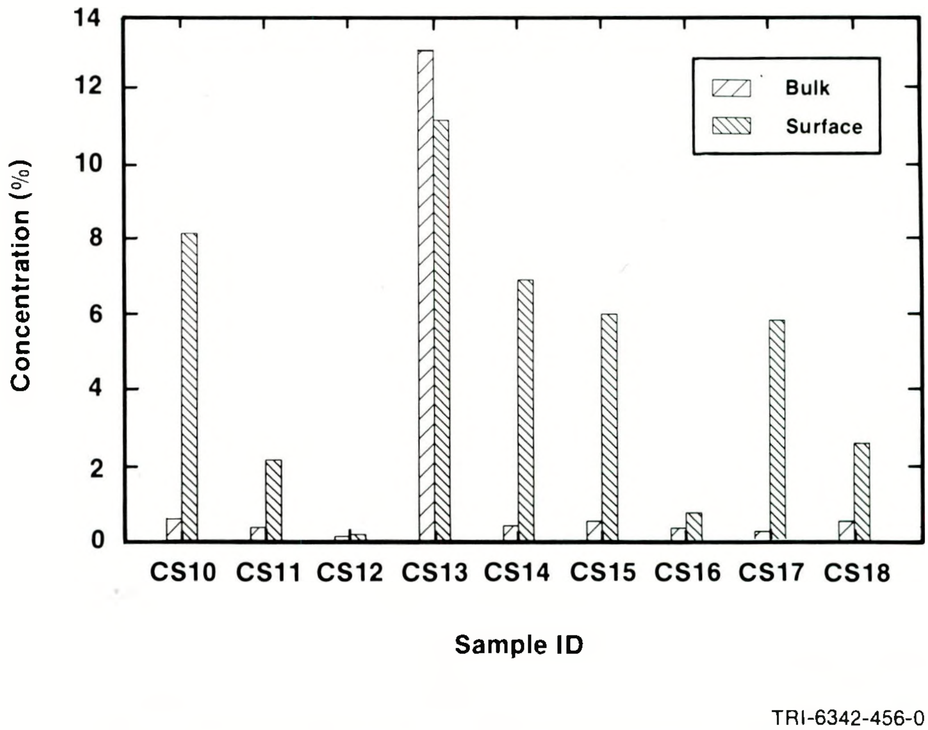

Figure V-4. Al_2O_3 Concentrations of CS10 through CS18.

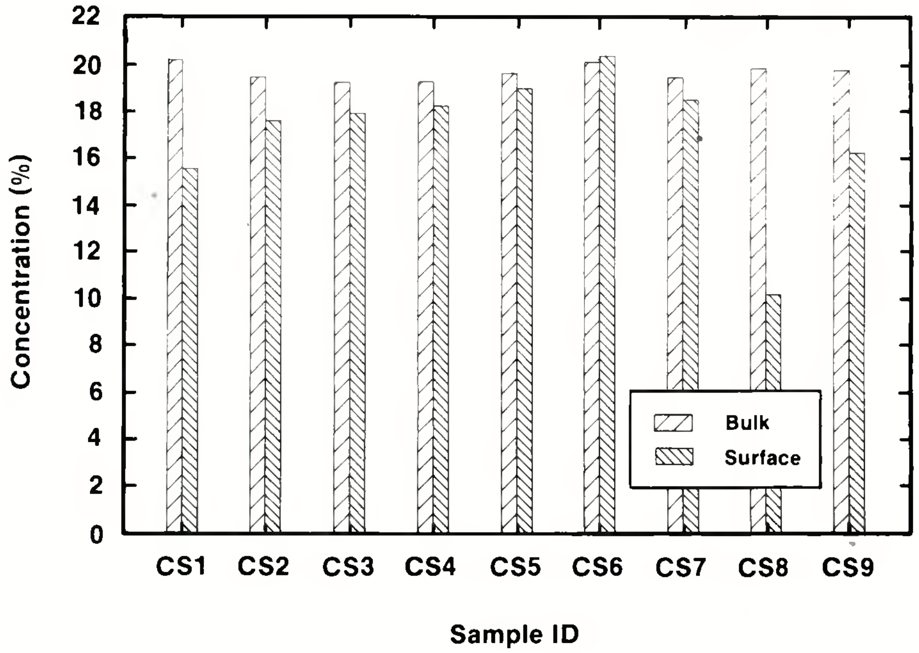

TRI-6342-457-0

Figure V-5. MgO Concentrations of CS1 through CS9.

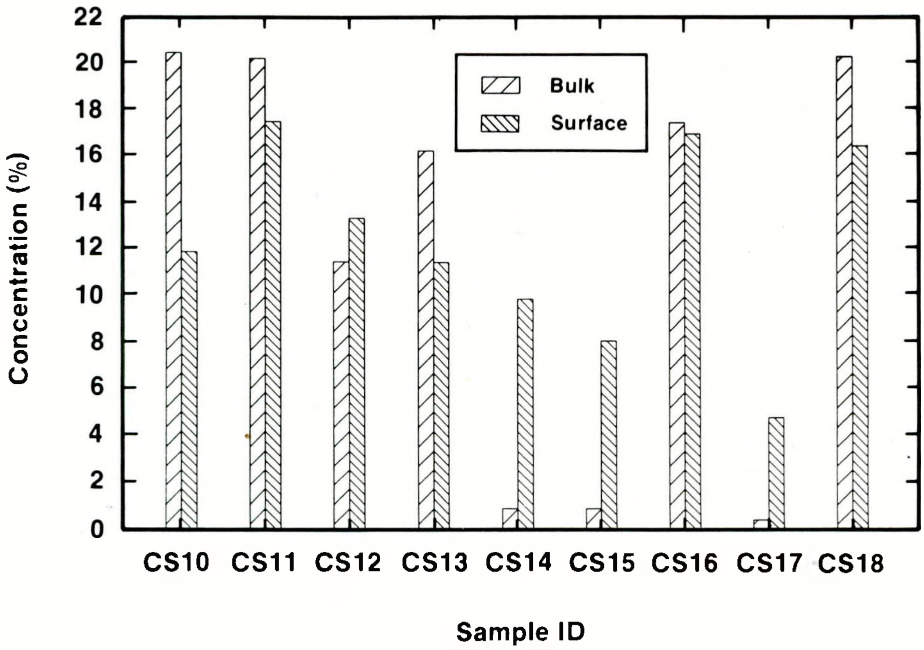

TRI-6342-458-0

Figure V-6. MgO Concentrations of CS10 through CS18.

surface, and this is generally the case, with a few exceptions, in which the bulk and surface concentrations are similar (Figures V-7 and V-8). In the two limestones, CS14 and CS15, the surface CaO is much lower in concentration than that in the bulk rock, and in the claystone (CS13), the surface mode is greater.

Fe_2O_3 is concentrated on the fracture surfaces in all samples except CS6, where they are nearly equal, and CS13, where the bulk rock concentration is higher. This trend closely follows that of the clay mineral modes (Figures V-9 and V-10), so it may be assumed that the concentration of Fe_2O_3 on the surface is due to the Fe_2O_3 content of the clay minerals.

K_2O is also concentrated on the fracture surfaces (Tables V-1 and V-2). This is also due to the higher clay mode on the surfaces, since illite is one of the components of the clay mineral assemblage (Sewards, Williams, and Keil, 1991), and illite typically contains about 7-8% K_2O.

Since the variation in composition is intimately associated with the variation in mineralogy, the above discussion may be more easily understood when the individual mineral modes are discussed in the following section.

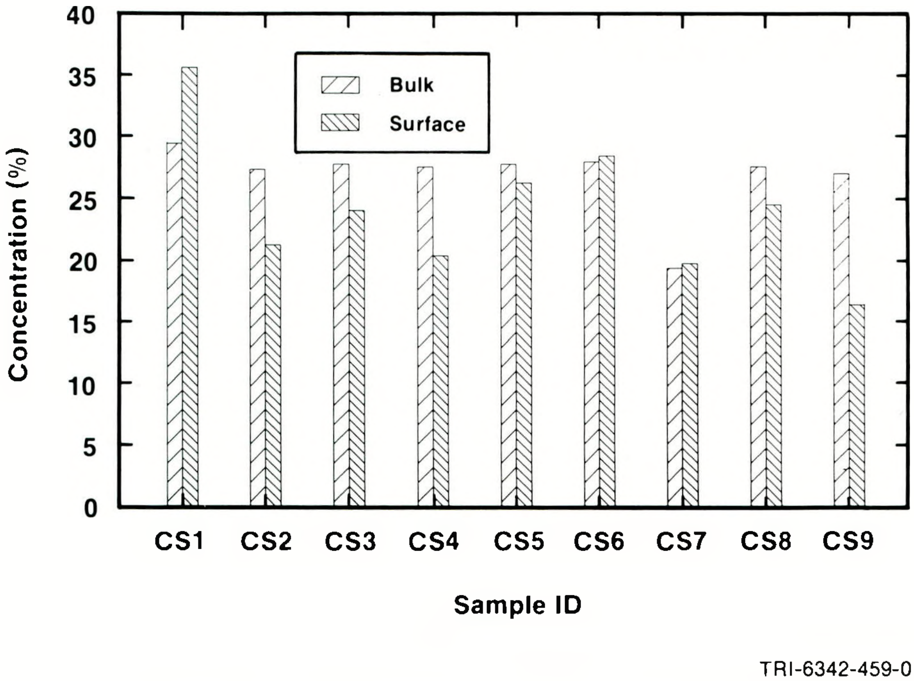

Figure V-7. CaO Concentrations of CS1 through CS9.

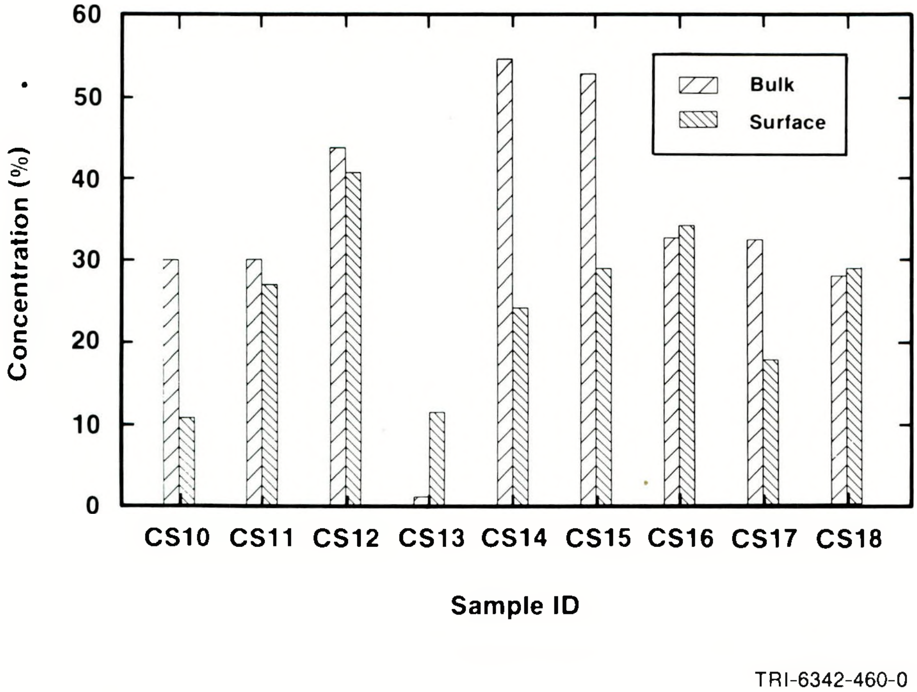

Figure V-8. CaO Concentrations of CS10 through CS18.

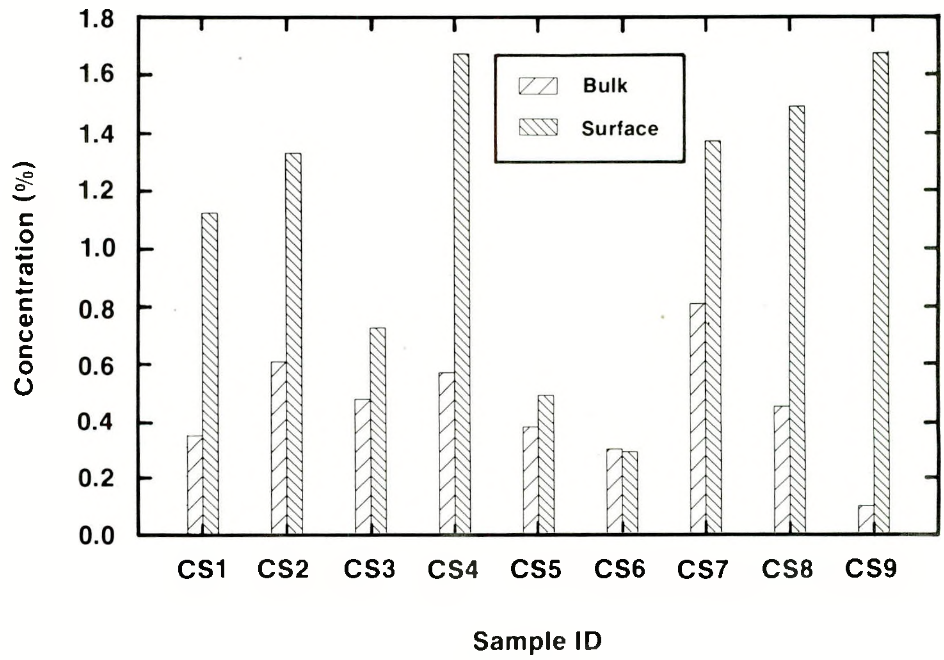

TRI-6342-461-0

Figure V-9. Fe_2O_3 Concentrations of CS1 through CS9.

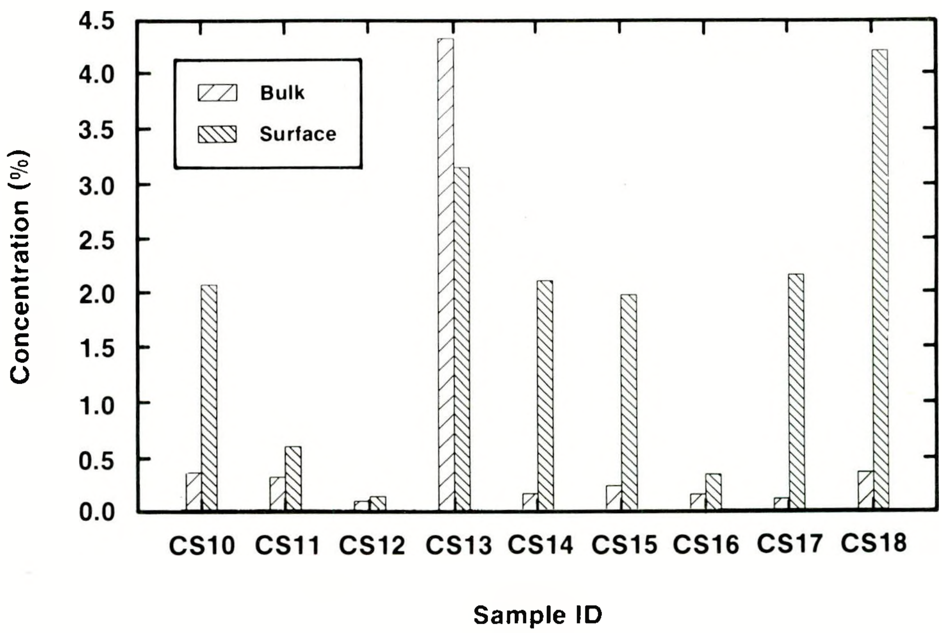

TRI-6342-462-0

Figure V-10. Fe_2O_3 Concentrations of CS10 through CS18.

VI. WHOLE ROCK AND FRACTURE SURFACE MINERALOGY

Table VI-1 lists the minerals that were identified in the bulk rock and fracture surfaces by XRD. These include dolomite, calcite, gypsum, halite, quartz, and clay. Halite in these samples is an artifact of the drilling process: a mixture of brine and mud was used to drill the wells; when the fluid evaporated, halite precipitated on the core surfaces.

The results of the whole rock and fracture surface mineral mode calculations, which are based on the compositional data included in the previous section, are listed in Tables VI-2 and VI-3. These tables are derived from Tables C-3 and C-4, listed in Appendix C, by subtracting the halite modes and normalizing to 100%. The mineral mode calculation method is discussed in Appendix B.

Clay

The clay modes for the bulk rock and fracture surface scrapings are displayed in bar diagram form in Figures VI-1 and VI-2. With the exception of two samples, CS7, a clay-rich dolomite, and CS13, a claystone, fracture surface clay contents are considerably higher than those of the bulk rock. The average bulk rock clay mode for these samples is 4.6% (excluding CS7 and CS13), whereas the average mode in the fracture surface scrapings is 18%, nearly four times the bulk rock average.

The reason the clay modes in the fracture surface scrapings are so much higher than the bulk rock modes is that the fractures occur primarily along clay-rich seams, since these are the weakest layers in the rock. In sample CS13, a claystone, the surface mode is less than that of the bulk mode. This is due to the fact that secondary calcite has been deposited on the fracture surface (Figure VI-7). Similarly, in sample CS7, the bulk clay mode is greater than the mode in the fracture surface scrapings because the fracture occurred along a quartz-rich layer (Figure VI-3).

Quartz

The quartz modes follow approximately the same trend as the clay modes: quartz modes in the fracture surface scrapings are substantially greater than those of the bulk rock (Figures VI-3 and VI-4). The zero values for the modes in the fracture surface scrapings in samples CS1 and CS3 in Figure VI-3 are due to the fact that there was insufficient sample to determine SiO_2 in these samples (Table VI-2).

Table VI-1. Semi-Quantitative Mineral Modes Determined by XRD

Sample ID	Well	Depth	Bulk						Surface					
			Evaporite Minerals				Clastic Minerals		Evaporite Minerals				Clastic Minerals	
			Dolomite	Calcite	Gypsum	Halite	Quartz	Clay	Dolomite	Calcite	Gypsum	Halite	Quartz	Clay
CS1	WIPP-12	838.6	****				*	*	**		**	****	**	**
CS2	WIPP-13	712.3	****				*	*	****		***	*	**	**
CS3	WIPP-13	705.3	****				*	*	****		*	***	**	**
CS4	WIPP-13	714.0	****				*	*	****		**	***	**	**
CS5	WIPP-26	187.5	****				*	*	****		*	**	**	**
CS6	WIPP-27	305.0	****				*	*	****			**	*	*
CS7	WIPP-28	447.5	****				**	**	****			**	**	**
CS8	WIPP-29	27.0	****				*	*	***		****	****	*	*
CS9	WIPP-30	633.5	****			*	**	**	****		**	**	***	**
CS10	WIPP-30	639.0	****				*	*	**		**	*	****	****
CS11	WIPP-30	635.0	****				*	*	***	*	**	****	**	**
CS12	WIPP-32	57.0	***	***	**		*	*	****	****		*	*	*
CS13	WIPP-32	91.1					****	****		***			****	****
CS14	WIPP-32	55.0		****			*	*		****			**	**
CS15	WIPP-32	56.0		****						****			**	**
CS16	WIPP-32	62.0	****	**					****	***			**	**
CS17	WIPP-33	570.0			****		*	*			****		***	**
CS18	WIPP-34	836.0	****				*	*	**		**	****	*	*

**** = Very abundant ** = Present
*** = Abundant * = Trace

Table VI-2. Bulk Rock Mineral Modes (Normalized to 100%)

Sample ID	Dolomite	Calcite	Gypsum	Halite	Clay	Quartz	Total
CS1B	97.85				1.61	0.54	100.00
CS2B	90.91				7.73	1.35	100.00
CS3B	92.26				6.59	1.14	100.00
CS4B	90.38				7.57	2.05	100.00
CS5B	94.66				4.49	0.86	100.00
CS6B	96.40				2.87	0.73	100.00
CS7B	58.62				34.66	6.72	100.00
CS8B	93.05				5.76	1.19	100.00
CS9B	77.26			0.83	16.83	5.08	100.00
CS10B	95.46				3.56	0.98	100.00
CS11B	97.48				2.19	0.34	100.00
CS12B	59.47	39.56	0.26		0.67	0.04	100.00
CS13B	3.03				83.77	13.20	100.00
CS14B	0.00	96.46			2.52	1.03	100.00
CS15B	0.00	95.19			3.38	1.44	100.00
CS16B	89.90	7.40			2.13	0.57	100.00
CS17B	0.00		97.40		1.58	1.02	100.00
CS18B	95.56				3.48	0.96	100.00

Table VI-3. Fracture Surface Mineral Modes (Normalized to 100%)

Sample ID	Dolomite	Calcite	Gypsum	Clay	Quartz	Total
CS1S	25.01		43.31	31.68	0.00	100.00
CS2S	60.18		0.86	26.45	12.51	100.00
CS3S	81.78		0.00	18.22	0.00	100.00
CS4S	59.45		2.64	25.39	12.53	100.00
CS5S	82.73		0.00	8.48	8.79	100.00
CS6S	93.06			3.86	3.08	100.00
CS7S	58.48			26.97	14.55	100.00
CS8S	43.72		33.95	12.08	10.25	100.00
CS9S	45.69		0.47	35.01	18.83	100.00
CS10S	27.89		0.00	43.49	28.62	100.00
CS11S	71.81	3.68	6.44	12.47	5.60	100.00
CS12S	65.19	33.04		0.90	0.87	100.00
CS13S		14.86		54.99	30.14	100.00
CS14S		37.46		40.06	22.48	100.00
CS15S		44.99		34.89	20.12	100.00
CS16S	78.41	13.32		4.37	3.90	100.00
CS17S			41.17	35.22	23.62	100.00
CS18S	78.56		0.00	14.17	7.27	100.00

Dolomite

In the samples containing dolomite, the fracture surfaces have less dolomite than the bulk rock, except for sample CS12, where the fracture surface has slightly more (Figures VI-5 and VI-6). In sample CS1, the mode in the fractures surface scrapings is only about 1/3 of the bulk mode; this is due to two factors: the mode in the fracture surface scrapings in this sample is considerably greater than the bulk mode (about 25% vs. 1.6%), and there is about 40% gypsum on the fracture surface. This gypsum is obviously of secondary origin, since the bulk gypsum mode is zero. Sample CS8 is very similar: the dolomite mode in the fracture surface scrapings is about 1/2 of the bulk mode, while there is 12% clay and 34% gypsum on the fracture surface.

Calcite

Calcite only appears in samples CS11 through CS16 (Figure VI-7). With the exception of CS11 (depth 635′), all these samples are from shallow cores (55′ to 92′ depth). In samples CS11 and CS13, in which the bulk calcite mode is zero, calcite in the fracture surface scrapings is a secondary precipitate. In sample CS16, the mode in the surface scrapings is greater than the bulk mode, which would also indicate secondary precipitation. In the remaining three samples, calcite in the bulk rock appears to have recrystallized from dolomite (see Chapter IV), and the fracture surfaces contain less calcite than the bulk rock. As in the dolomite samples, this is due to the fact that the fractures occurred along clay- and quartz-rich seams.

Gypsum

With the exception of sample CS17, which is massive gypsum, gypsum only appears in the fracture surface modes (samples CS1, CS2, CS4, CS8, CS9, and CS11) (Figures VI-8 and VI-9). Clearly, the gypsum precipitated from solution on the fracture surfaces in these samples. In sample CS17, the surface mode is much lower than the bulk mode. Again, it appears that the fracture surface occurred along a clay-rich vein, since the surface clay mode is 35%.

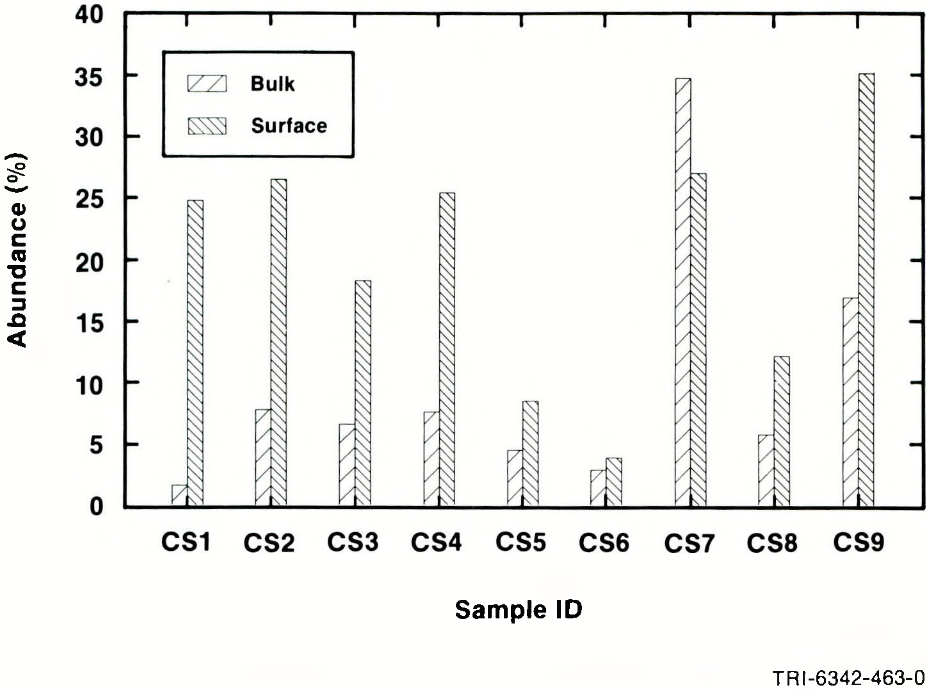

Figure VI-1. Clay Modes of CS1 through CS9.

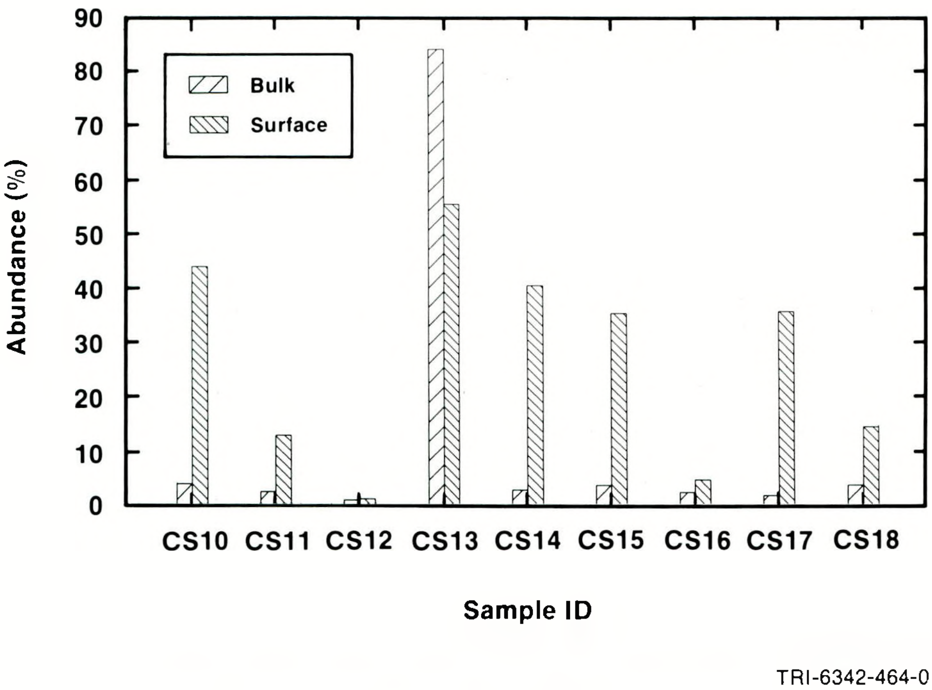

Figure VI-2. Clay Modes of CS10 through CS18.

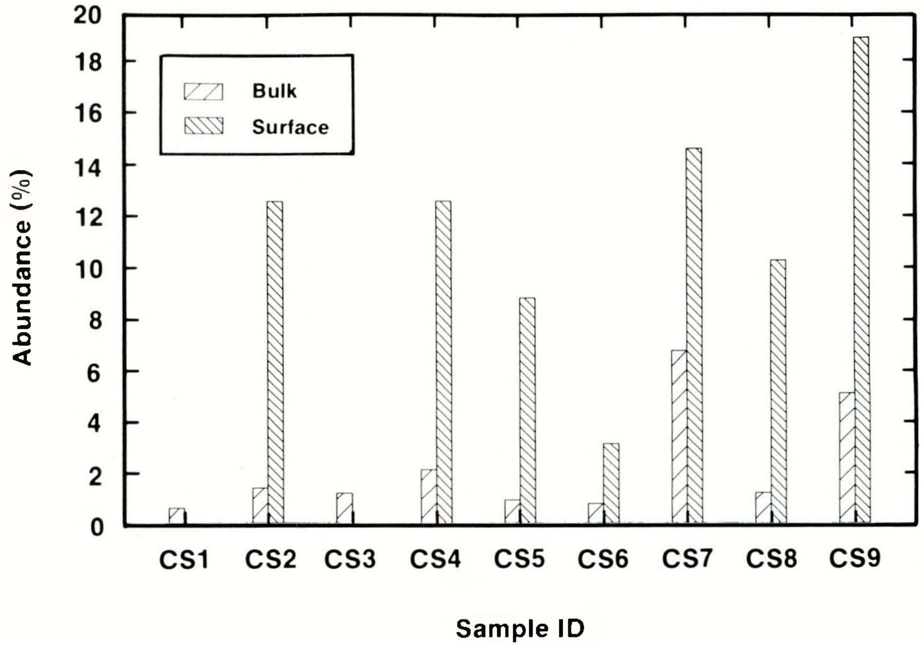

TRI-6342-465-0

Figure VI-3. Quartz Modes of CS1 through CS9.

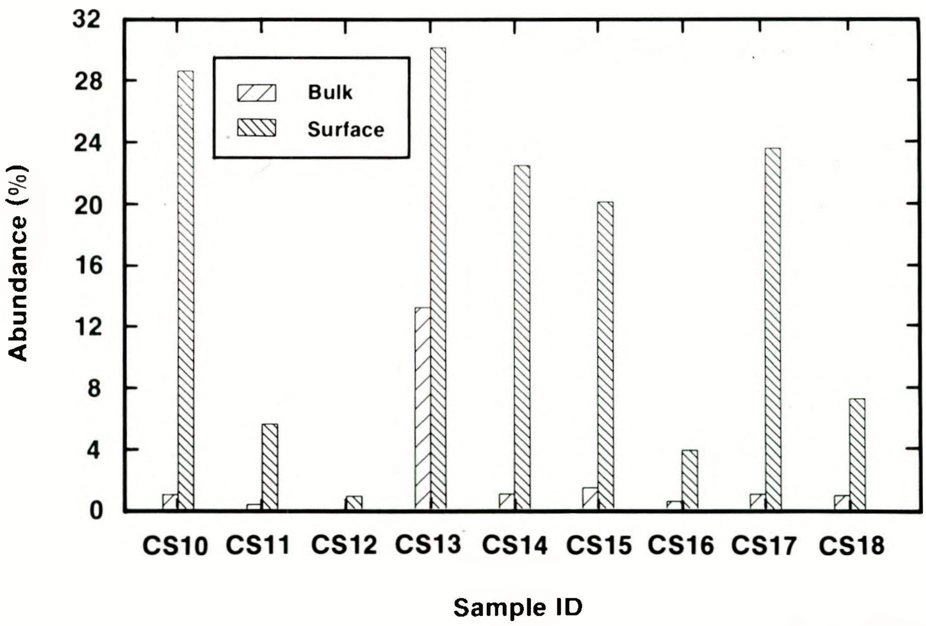

TRI-6342-466-0

Figure VI-4. Quartz Modes of CS10 through CS18.

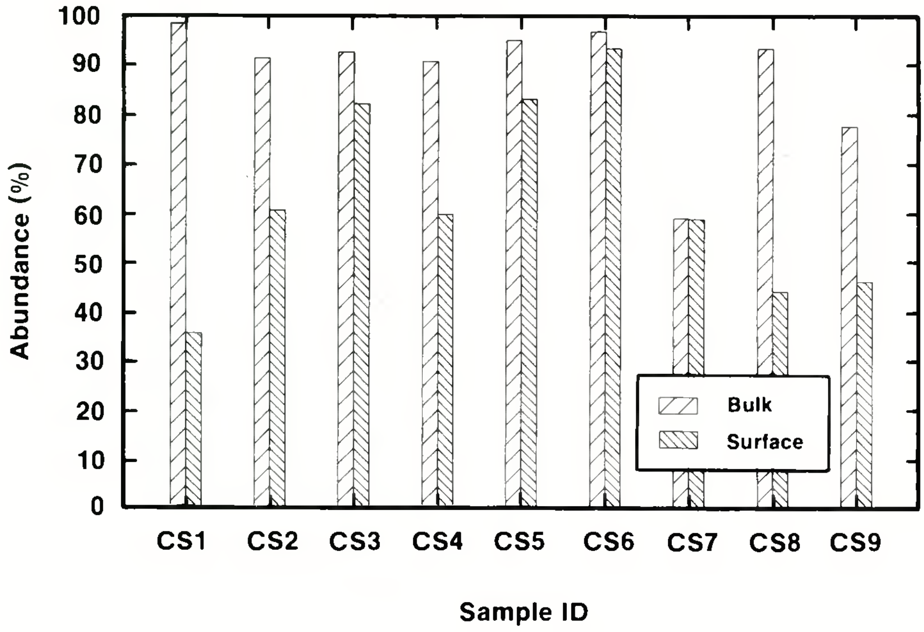

TRI-6342-467-0

Figure VI-5. Dolomite Modes of CS1 through CS9.

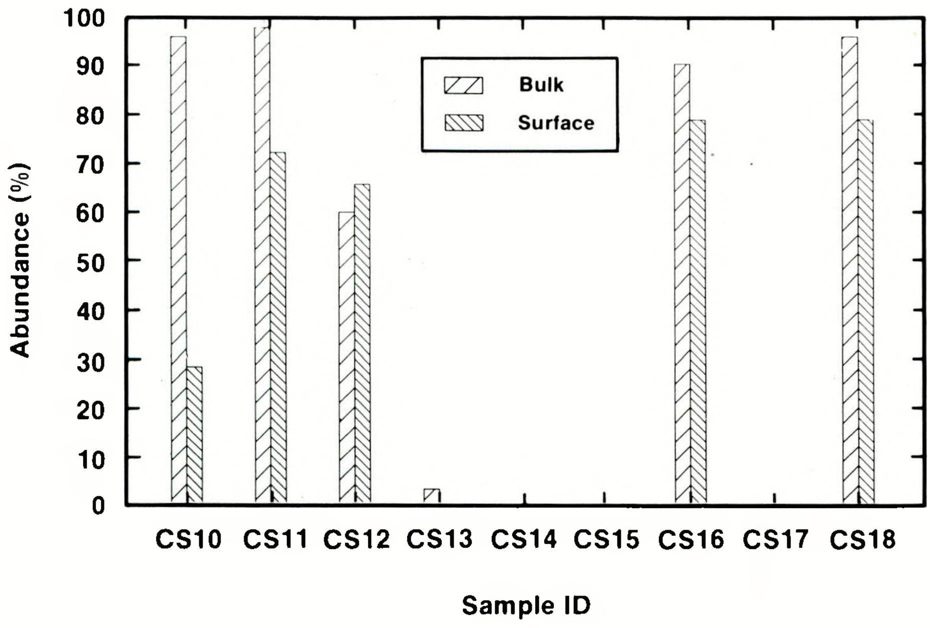

TRI-6342-468-0

Figure VI-6. Dolomite Modes of CS10 through CS18.

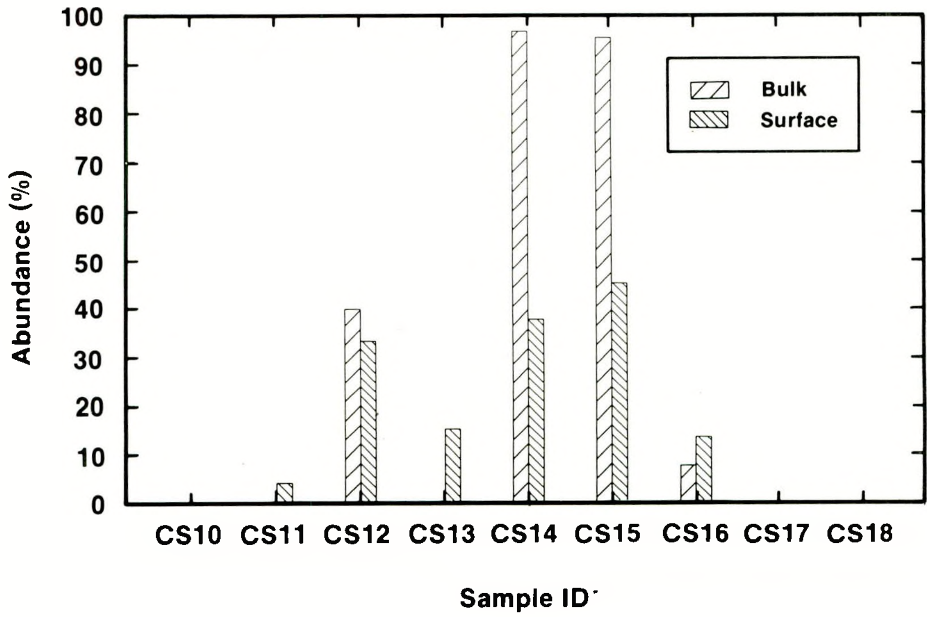

TRI-6342-469-0

Figure VI-7. Calcite Modes of CS10 through CS18.

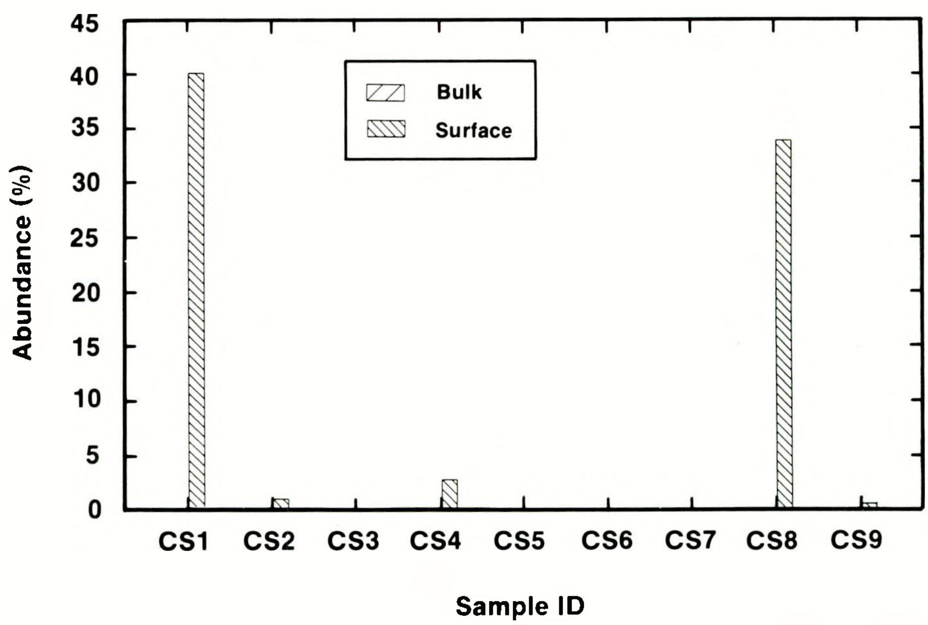

TRI-6342-470-0

Figure VI-8. Gypsum Modes of CS1 through CS9.

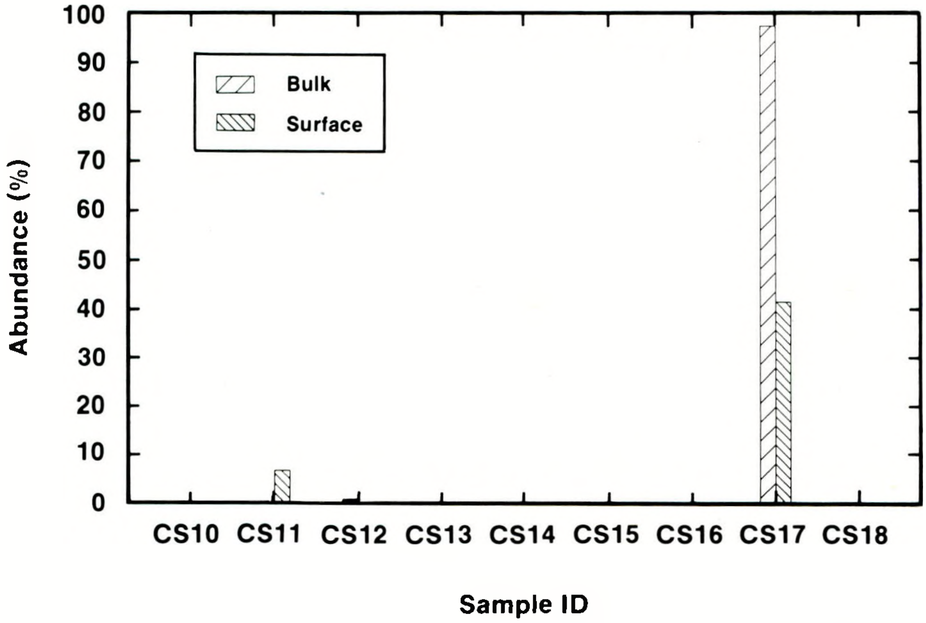

TRI-6342-471-0

Figure VI-9. Gypsum Modes of CS10 through CS18.

VII. DOLOMITE COMPOSITIONS

Compositions of dolomite grains on a fracture surface were obtained on the electron microprobe for only one sample, CS4. Other thin sections, in which the fracture surface rim was not destroyed by the polishing process, did not yield good totals (51.1% for an ideal dolomite) because the dolomite grains were either too small or were intermixed with clay. Table VII-1 shows the results for sample CS4. The difference between the compositions of the dolomite grains on the fracture surface and those in the bulk rock is insignificant. They are also very similar to those of other Culebra Dolomite samples (Sewards, Williams, and Keil, 1991). Clearly, the compositions of the dolomite grains in this sample were not affected by fluid moving in the fractures.

Table VII-1. Dolomite Compositions, Sample CS4

	Bulk							
	Oxides				Cations			
#	CaO	FeO	MgO	Total	Ca	Fe	Mg	Total
1	25.80	0.20	18.44	44.44	1.000	0.006	0.994	2.000
2	30.89	0.10	20.75	51.74	1.032	0.003	0.965	2.000
3	28.40	0.20	19.69	48.29	1.015	0.006	0.979	2.000
4	29.78	0.15	21.53	51.46	0.995	0.004	1.001	2.000
5	30.34	0.05	20.70	51.09	1.025	0.001	0.973	2.000
6	28.92	0.00	20.14	49.06	1.016	0.000	0.984	2.000
7	28.85	0.38	19.28	48.51	1.031	0.011	0.959	2.000
8	30.99	0.00	20.49	51.48	1.042	0.000	0.958	2.000
9	29.17	0.00	20.47	49.64	1.012	0.000	0.988	2.000
10	28.38	0.19	20.62	49.19	0.992	0.005	1.003	2.000
11	29.44	0.10	19.43	48.97	1.041	0.003	0.956	2.000
12	29.99	0.00	18.99	48.98	1.063	0.000	0.937	2.000
					1.022	0.003	0.975	2.000

	Surface							
	Oxides				Cations			
#	CaO	FeO	MgO	Total	Ca	Fe	Mg	Total
1	29.81	0.00	19.87	49.68	1.038	0.000	0.962	2.000
2	27.41	0.00	18.87	46.28	1.021	0.000	0.979	2.000
3	28.70	0.00	20.03	48.73	1.015	0.000	0.985	2.000
4	27.36	0.00	17.52	44.88	1.058	0.000	0.942	2.000
5	28.80	0.00	20.06	48.86	1.016	0.000	0.984	2.000
6	29.75	0.00	20.81	50.56	1.013	0.000	0.987	2.000
7	27.63	0.00	19.84	47.47	1.000	0.000	1.000	2.000
8	27.54	0.43	19.53	47.50	1.000	0.012	0.987	2.000
9	28.25	0.52	19.76	48.53	1.006	0.014	0.979	2.000
10	29.49	0.34	19.68	49.51	1.032	0.009	0.959	2.000
11	28.03	0.10	17.83	45.96	1.059	0.003	0.938	2.000
12	30.20	0.15	20.89	51.24	1.017	0.004	0.979	2.000
					1.023	0.004	0.973	2.000

VIII. DISCUSSION

Two main conclusions can be drawn from the information presented above: (1) horizontal water-bearing fractures in dolomite and calcite rock tend to occur in zones where clay and quartz are concentrated, particularly along clay seams, and (2) secondary minerals, primarily gypsum and some calcite, are precipitated from solution onto the fracture surfaces. The clay modes in fracture surface scrapings in dolomite rock range from about 1% to 43%, with an average of 18%, whereas clay modes in the bulk rock in these samples range from less than 1% to 7%, with an average of 4.6%. Similarly, for the two limestone samples, the clay mode is much greater on the fracture surface than in the bulk rock (37% vs. 2%). Secondary gypsum is an important constituent of the fracture surface mineralogy in these samples. Secondary calcite is present in only one sample from a deep core and all five shallow cores.

Dolomite compositions on the fracture surfaces are no different from those in the bulk rock, indicating that aqueous alteration of dolomite did not occur to any significant extent (with the possible exception of some dissolution and recrystallization.

Where present, calcite in these samples, both in the bulk rock and fracture surfaces, is a product of recrystallization from dolomite caused by aqueous alteration, usually near surface.

It should be mentioned that the surfaces examined in this study are all due to horizontal fractures; no surfaces of vertical or high-angle fractures that were clearly identifiable as water-bearing were discovered in the cores examined. It is probable that the vertical and near-vertical fracture surfaces are not as clay-rich as the horizontal ones, since accumulations of clay occur along horizontal planes due to sedimentation.

The implications of these results for the WIPP repository are obvious: since the cation exchange capacity of clay minerals is so much higher than that of dolomite, calcite, or gypsum, and the clay minerals are a major component of the fracture surface mineralogy, the sorption of radionuclides due to the clay will far outweigh that of the other minerals. This fact should be taken into account in any study of the transport of radionuclides through the Culebra Dolomite.

IX. REFERENCES

Borns, D.J., L.J. Barrows, D.W. Powers, and R.P. Snyder. 1982. *Deformation of Evaporites Near the Waste Isolation Pilot Plant (WIPP) Site*. SAND82-1069. Albuquerque, NM: Sandia National Laboratories.

Ferrall, C.C., and J.F. Gibbons. 1979. *Core Study of the Rustler Formation Over the WIPP Site*. SAND79-7110. Albuquerque, NM: Sandia National Laboratories.

Sewards, T., R. Glenn, and K. Keil. 1991. *Mineralogy of the Rustler Formation in the WIPP-19 Core*. SAND87-7036. Albuquerque, NM: Sandia National Laboratories.

Sewards, T., M. Williams, and K. Keil. 1991. *Mineralogy of the Culebra Dolomite Member of the Rustler Formation*. SAND90-7008. Albuquerque, NM: Sandia National Laboratories.

APPENDIX A:
ANALYTICAL PROCEDURES

X-Ray Diffraction Analysis

Small portions of the ground and sieved whole rock and fracture surface powders were placed in Plexiglas containers (2.5 x 2.5 x 0.4 cm), which have a 1 mm deep hollowed-out compartment. The surface of the powder was then scraped off level with the top surface of the Plexiglas container. The container was placed in the sample holder of a Scintag PAD-V automated diffractometer and analyzed from 2° 2-θ to 60° 2-θ at a scanning rate of 3° per minute using a 0.03° chopper increment.

X-Ray Fluorescence Analysis

Whole rock samples were ground with a mortar and pestle and then passed through a 100 mesh sieve. Fused glass disks were prepared according to standard procedures (Norrish and Chappell, 1967) and analyzed on a Rigaku 3064M x-ray fluorescence spectrometer for 10 elements: SiO_2, Al_2O_3, TiO_2, Fe_2O_3, MnO, MgO, CaO, Na_2O, K_2O, and P_2O_5. Four standards were used: (1) NBS-88b (National Bureau of Standards - Dolomitic Limestone); (2) BCS-CRM-393 (British Chemical Standard - Chemical Reference Material); (3) Dol-1 (Echantillon-type de Calcite), and (4) AM-PAD44 (Amostra Pedrao 44).

Atomic Absorption Spectroscopy

Fracture surface samples were ground and sieved, dissolved in hydrofluoric and perchloric acid mixture, and analyzed on a Perkin-Elmer 303 atomic absorption spectrophotometer for seven elements: SiO_2, Al_2O_3, Fe_2O_3, MgO, CaO, Na_2O, and K_2O (McLaughlin, 1967).

Electron Microprobe Elemental Analysis

Polished thin sections of the samples were prepared using no water and maintaining a temperature below 60°C. The sections were coated with carbon in a vacuum evaporator. Mineral grains were analyzed with a JEOL 733 electron microprobe using an acceleration potential of 15KV, a beam current of 2 nanoamperes, a beam diameter of 1.5 microns, for a period of 80 seconds per analysis. Analyses were corrected according to standard Bence-Albee procedures.

Appendix A References

McLaughlin, R.J.W. 1967. "Atomic Absorption Spectroscopy." *Physical Methods in Determinative Mineralogy*, J. Zussman, ed. Academic Press, 514p.

Norrish, K., and B.W. Chappell. 1967. "X-ray Fluorescence Spectrography." *Physical Methods in Determinative Mineralogy*, J. Zussman, ed. Academic Press, 514p.

APPENDIX B: MODAL MINERALOGICAL CALCULATIONS

Modes for the minerals identified by x-ray diffraction (XRD) were determined from the compositional data obtained by x-ray fluorescence (XRF) and atomic absorption (AA). Based on the compositions of the individual minerals, a particular element, when present in only one mineral, was used to determine the mode of that mineral. For example, the only phase containing aluminum in these samples is clay, and electron microprobe analyses of clay samples from the Culebra Dolomite (Sewards, Williams, and Keil, 1991) show that the clay aggregates contain an average of 15% Al_2O_3; thus, the weight percent of clay is calculated according to the formula:

$$Clay(wt\%) = Al_2O_3 / 0.15$$

Quartz, since it contains only SiO_2, is determined by:

$$Quartz(wt\%) = SiO_2 - Clay(wt\%) \times 0.46$$

since the average SiO_2 content of the clay fraction is 46%. The remaining mineral modes are determined using the following formulae:

$$Dolomite(wt\%) = (MgO - Clay \times 0.15) / 0.19$$

or: $$Dolomite(wt\%) = (CaO - Gypsum \times 0.336) / 0.304$$

$$Gypsum(wt\%) = SO_3 / 0.465$$

or: $$Gypsum(wt\%) = (CaO - Dolomite(wt\%) \times 0.304) / 0.326$$

$$Calcite(wt\%) = (CaO - Dolomite \times 0.304) / 0.56$$

Appendix B Reference

Sewards, T., M. Williams, and K. Keil. 1991. *Mineralogy of the Culebra Dolomite Member of the Rustler Formation.* SAND90-7008. Albuquerque, NM: Sandia National Laboratories.

APPENDIX C:
DATA TABLES

Tables C-1 and C-2 are the raw data from the bulk rock and fracture surface compositional analyses. Tables V-1 and V-2 are derived from these by converting the Na_2O data to NaCl, subtracting this, and normalizing. Similarly, Tables C-3 and C-4 are the results of the mineral mode calculations from Tables C-1 and C-2. Tables VI-2 and VI-3 are derived from these by removing the halite modes and normalizing to 100%.

Table C-1. Bulk Rock Compositions

Sample ID	Well	Depth	SiO_2	TiO_2	Al_2O_3	Fe_2O_3	MnO	MgO	CaO	Na_2O	K_2O	P_2O_5	SO_3	Total
CS1B	WIPP-12	838.60	1.27	0.02	0.24	0.34	0.03	20.22	29.50	0.07	0.07	0.04	0.16	51.94
CS2B	WIPP-13	712.30	4.87	0.08	1.15	0.60	0.02	19.50	27.40	0.04	0.37	0.04	0.07	54.13
CS3B	WIPP-13	705.30	4.14	0.06	0.98	0.47	0.03	19.27	27.80	0.06	0.31	0.04	0.07	53.23
CS4B	WIPP-13	714.00	5.56	0.05	1.14	0.56	0.02	19.30	27.60	0.05	0.37	0.04	0.04	54.72
CS5B	WIPP-26	187.50	2.82	0.04	0.65	0.37	0.04	19.65	27.80	0.07	0.29	0.04	0.05	51.81
CS6B	WIPP-27	305.00	1.95	0.03	0.41	0.29	0.02	20.05	27.90	0.25	0.24	0.05	0.09	51.28
CS7B	WIPP-28	447.50	24.02	0.29	5.51	0.78	0.03	19.02	18.89	1.29	1.19	0.03	0.10	71.15
CS8B	WIPP-29	27.00	3.73	0.06	0.84	0.44	0.02	19.80	27.50	0.22	0.34	0.05	0.06	53.05
CS9B	WIPP-30	633.50	14.27	0.17	2.81	0.09	0.01	19.15	26.14	1.75	1.12	0.13	0.19	65.83
CS10B	WIPP-30	639.00	2.70	0.04	0.55	0.34	0.02	20.40	29.90	0.05	0.18	0.10	0.05	54.32
CS11B	WIPP-30	635.00	1.35	0.02	0.33	0.30	0.02	20.05	29.80	0.30	0.13	0.10	0.07	52.46
CS12B	WIPP-32	57.00	0.35	0.01	0.10	0.08	0.01	11.40	43.60	0.05	0.02	0.18	0.12	55.92
CS13B	WIPP-32	91.10	53.36	0.74	12.96	4.32	0.01	16.15	0.95	0.05	2.32	0.21	0.03	91.10
CS14B	WIPP-32	55.00	2.20	0.02	0.38	0.15	0.02	0.84	54.40	0.04	0.13	0.25	0.13	58.56
CS15B	WIPP-32	56.00	2.95	0.03	0.50	0.22	0.02	0.84	52.60	0.04	0.17	0.25	0.12	57.73
CS16B	WIPP-32	62.00	1.55	0.02	0.32	0.14	0.01	17.40	32.50	0.05	0.12	0.12	0.07	52.30
CS17B	WIPP-33	570.00	1.77	0.02	0.24	0.10	0.00	0.35	32.20	0.10	0.04	N.A.	45.97	80.79
CS18B	WIPP-34	836.00	2.45	0.04	0.50	0.34	0.02	20.20	27.80	0.06	0.18	0.10	0.09	51.77

Table C-2. Fracture Surface Compositions

Sample ID	Well	Depth	SiO_2	Al_2O_3	Fe_2O_3	MgO	CaO	Na_2O	K_2O	SO_3	Total
CS1S	WIPP-12	838.60	*	2.80	0.40	5.60	12.80	34.00	0.32	*	55.52
CS2S	WIPP-13	712.30	15.90	4.40	1.28	17.08	20.60	1.68	1.19	*	60.85
CS3S	WIPP-13	705.30	*	2.10	0.56	14.04	18.80	11.60	0.82	*	47.36
CS4S	WIPP-13	714.00	15.60	4.16	1.50	16.50	18.40	5.16	0.12	1.34	61.28
CS5S	WIPP-26	187.50	9.58	1.30	0.44	17.36	24.00	4.66	0.57	*	57.47
CS6S	WIPP-27	305.00	3.46	0.60	0.26	18.90	26.40	3.92	0.29	*	53.57
CS7S	WIPP-28	447.50	18.90	4.66	1.28	17.46	18.60	3.08	0.87	0.03	63.60
CS8S	WIPP-29	27.00	7.10	1.16	0.94	6.48	15.60	19.30	0.79	*	50.43
CS9S	WIPP-30	633.50	23.30	5.76	1.56	15.28	15.40	3.24	1.83	*	64.81
CS10S	WIPP-30	639.00	38.20	7.88	2.00	11.48	10.24	1.58	2.09	*	71.47
CS11S	WIPP-30	635.00	4.49	1.30	0.36	10.78	16.60	20.28	0.38	2.08	55.91
CS12S	WIPP-32	57.00	0.96	0.14	0.12	12.94	39.60	1.26	0.06	0.02	54.98
CS13S	WIPP-32	91.10	45.50	11.06	3.12	11.30	11.16	0.34	1.56	0.29	81.21
CS14S	WIPP-32	55.00	28.40	6.76	2.06	9.64	23.60	0.96	1.80	0.01	71.17
CS15S	WIPP-32	56.00	25.40	5.90	1.94	7.90	28.40	0.70	1.33	0.01	69.64
CS16S	WIPP-32	62.00	4.48	0.70	0.32	16.60	33.40	0.98	0.24	0.60	57.00
CS17S	WIPP-33	570.00	28.30	5.74	2.12	4.64	17.40	0.72	1.29	20.80	78.89
CS18S	WIPP-34	836.00	2.64	0.68	1.12	4.36	7.64	38.90	0.18	*	54.40

* = Insufficient Sample

Table C-3. Bulk Rock Mineral Modes (Unnormalized)

Sample ID	Dolomite	Calcite	Gypsum	Halite	Clay	Quartz	Total
CS1B	97.04				1.60	0.53	99.17
CS2B	90.13				7.67	1.34	99.14
CS3B	91.45				6.53	1.13	99.12
CS4B	90.79				7.60	2.06	100.45
CS5B	91.45				4.33	0.83	96.61
CS6B	91.78				2.73	0.69	95.20
CS7B	62.14				36.73	7.12	105.99
CS8B	90.46				5.60	1.15	97.21
CS9B	85.99			0.93	18.73	5.65	111.30
CS10B	98.36				3.67	1.01	103.04
CS11B	98.03				2.20	0.34	100.56
CS12B	59.47	39.56	0.26		0.67	0.04	100.00
CS13B	3.13				86.40	13.62	103.14
CS14B		97.14			2.53	1.03	100.71
CS15B		93.93			3.33	1.42	98.68
CS16B	89.89	7.40			2.13	0.57	100.00
CS17B			98.86		1.60	1.03	101.49
CS18B	91.45				3.33	0.92	95.70

Table C-4. Fracture Surface Mineral Modes (Unnormalized)

Sample ID	Dolomite	Calcite	Gypsum	Halite	Clay	Quartz	Total
CS1S	14.74		25.52	64.09	18.67	0.00	123.01
CS2S	66.74		0.96	3.17	29.33	13.88	114.07
CS3S	62.84		0.00	21.87	14.00	0.00	98.71
CS4S	64.95		2.88	9.73	27.73	13.69	118.98
CS5S	84.53		0.00	8.78	8.67	8.98	110.96
CS6S	96.32			7.39	4.00	3.18	110.89
CS7S	67.37			5.81	31.07	16.76	121.00
CS8S	28.00		21.74	36.38	7.73	6.57	100.42
CS9S	50.11		0.52	6.11	38.40	20.65	115.78
CS10S	33.68		0.00	2.98	52.53	34.58	123.77
CS11S	49.89	2.56	4.47	38.23	8.67	3.89	107.71
CS12S	67.37	34.14		2.38	0.93	0.90	105.72
CS13S		19.93		0.64	73.73	40.41	134.72
CS14S		42.14		1.81	45.07	25.29	114.31
CS15S		50.71		1.32	39.33	22.69	114.05
CS16S	83.68	14.21		1.85	4.67	4.16	108.57
CS17S			44.73	1.36	38.27	25.66	110.02
CS18S	25.13		0.00	73.33	4.53	2.33	105.32

FEDERAL AGENCIES

U. S. Department of Energy, (5)
Office of Civilian Radioactive Waste
Management
Attn: Deputy Director, RW-2
Associate Director, RW-10
Office of Program Administration
and Resources Management
Associate Director, RW-20
Office of Facilities Siting
and Development
Associate Director, RW-30
Office of Systems Integration
and Regulations
Associate Director, RW-40
Office of External Relations
and Policy
Forrestal Building
Washington, DC 20585

U. S. Department of Energy (3)
Albuquerque Operations Office
Attn: J. E. Bickel
R. Marquez, Director
Public Affairs Division
P.O. Box 5400
Albuquerque, NM 87185

U. S. Department of Energy
Attn: National Atomic Museum Library
Albuquerque Operations Office
P. O. Box 5400
Albuquerque, NM 87185

U. S. Department of Energy (4)
WIPP Project Office (Carlsbad)
Attn: Vernon Daub
J. A. Mewhinney
P.O. Box 3090
Carlsbad, NM 88221

U. S. Department of Energy
Research & Waste Management Division
Attn: Director
P. O. Box E
Oak Ridge, TN 37831

U.S. Department of Energy
Richland Operations Office
Nuclear Fuel Cycle & Production Division
Attn: R. E. Gerton
P.O. Box 500
Richland, WA 99352

U. S. Department of Energy (1)
Attn: Edward Young
Room E-178
GAO/RCED/GTN
Washington, DC 20545

U. S. Department of Energy (6)
Office of Environmental Restoration
and Waste Management
Attn: Jill Lytle, EM30
Mark Frei, EM-34 (3)
Mark Duff, EM-34
Clyde Frank, EM-50
Washington, DC 20585

U. S. Department of Energy (3)
Office of Environment, Safety and Health
Attn: Ray Pelletier, EH-231
Kathleen Taimi, EH-232
Carol Borgstrom, EH-25
Washington, DC 20585

U. S. Department of Energy
Ecological Research Division, ER-75
Office of Health and Environmental Research
Office of Energy Research
Attn: F. J. Wobber
Washington, DC 20545

U. S. Department of Energy (2)
Idaho Operations Office
Fuel Processing and Waste
Management Division
785 DOE Place
Idaho Falls, ID 83402

U.S. Department of Energy
Savannah River Operations Office
Defense Waste Processing
Facility Project Office
Attn: W. D. Pearson
P.O. Box A
Aiken, SC 29802

U. S. Department of the Interior (5)
Attn: N. Trask (MS 410)
T. Coplen (MS 431)
B. F. Jones (MS 432)
L. N. Plummer (MS 432)
I. J. Winograd (MS 432)
Geological Survey
National Center
Reston, VA 22092

U. S. Department of the Interior
Attn: J. S. McLean
Geological Survey
Box 25046, MS406
Denver, CO 80225

U. S. Department of the Interior
Attn: J. Thomas
Geological Survey
705 N. Plaza Street
Carson City, NV 89701

U. S. Department of the Interior
Attn: Librarian
National Park Service
Carlsbad Caverns National Park
3225 National Parks Highway
Carlsbad, NM 88220

U. S. Environmental Protection Agency (4)
Attn: Ray Clark (2)
Mark Cotton (2)
Office of Radiation Programs (ANR-460)
Washington, DC 20460

U.S. Geological Survey
Branch of Regional Geology
Attn: R. Snyder
MS913, Box 25046
Denver Federal Center
Denver, CO 80225

U.S. Geological Survey
Conservation Division
Attn: W. Melton
P.O. Box 1857
Roswell, NM 88201

U.S. Geological Survey (4)
Water Resources Division
Attn: Kathy Peter (2)
Roger Ferriera
Scott Anderholm
Suite 200
4501 Indian School NE
Albuquerque, NM 87110

U.S. Nuclear Regulatory Commission (8)
Attn: Joseph Bunting, HLEN 4H3 OWFN
Ron Ballard, HLGP 4H3 OWFN
Michael Bell
David Brooks
Tin Mo
Jacob Philip
John Randall
NRC Library
Mail Stop 623SS
Washington, DC 20555

Office of Nuclear Regulatory Research (4)
U. S. Nuclear Regulatory Commission
MS: NL-005
Washington, DC 20555
Attn: G. F. Birchard
L. A. Kovach
T. J. Nicholson
J. D. Randall

Boards

Defense Nuclear Facilities Safety Board
Attn: Dermot Winters
Suite 675
600 E Street, NW
Washington, DC 20004

U. S. Department of Energy
Advisory Committee on Nuclear
Facility Safety
Attn: Merritt E. Langston, AC21
Washington, DC 20585

Nuclear Waste Technical
Review Board (2)
Attn: Dr. Don A. Deere
Dr. Sidney J. S. Parry
Suite 910
1100 Wilson Blvd.
Arlington, VA 22209-2297

Richard Major
Advisory Committee on Nuclear Waste
Nuclear Regulatory Commission
7920 Norfolk Avenue
Bethesda, MD 20814

STATE AGENCIES

Environmental Evaluation Group (3)
Attn: Library
Suite F-2
7007 Wyoming Blvd., N.E.
Albuquerque, NM 87109

New Mexico Bureau of Mines
and Mineral Resources (2)
Attn: F. E. Kottolowski, Director
J. Hawley
Socorro, NM 87801

NM Department of Energy & Minerals
Attn: Librarian
2040 S. Pacheco
Santa Fe, NM 87505

NM Environmental Improvement Division
Attn: Deputy Director
1190 St. Francis Drive
Santa Fe, NM 87503

LABORATORIES/CORPORATIONS

Battelle Pacific Northwest Laboratories (7)
Attn: D. J. Bradley, K6-24
J. Relyea, H4-54
R. E. Westerman, P8-37
K. Krupa, K2-57
H. C. Burkholder, P7-41
L. Pederson, K6-47
J. Serne
Battelle Boulevard
Richland, WA 99352

Geohydrology Associates
Attn: T. E. Kelly
4015 Carlisle Blvd NE
Albuquerque, NM 87110

Savannah River Laboratory (6)
Attn: N. Bibler
E. L. Albenisius
M. J. Plodinec
G. G. Wicks
C. Jantzen
J. A. Stone
Aiken, SC 29801

George Dymmel
SAIC
101 Convention Center Dr.
Las Vegas, NV 89109

INTERA Inc. (3)
Attn: G. E. Grisak
J. F. Pickens
A. Haug
Suite #300
6850 Austin Center Blvd.
Austin, TX 78731

INTERA Inc.
Attn: Wayne Stensrud
P.O. Box 2123
Carlsbad, NM 88221

INTERA Inc.
Attn: A. Marsh LaVenue
8100 Mountain Road
Suite #204D
Albuquerque, NM 87110

IT Corporation (3)
Attn: R. F. McKinney
J. Myers
R. Holt
Regional Office - Suite 700
5301 Central Avenue, NE
Albuquerque, NM 87108

IT Corporation (2)
Attn: D. E. Deal
P.O. Box 2078
Carlsbad, NM 88221

Arthur D. Little, Inc. (3)
Attn: C. R. Hadlock
Scot Foster
Philip Rury
Acorn Park
Cambridge, MA 02140-2390

Los Alamos National Laboratory (10)
Attn: A. Meijer
D. Broxton
B. Carlos
D. Eggert
D. Hobart
E. Springer
I. Triay
J. F. Kerrisk
D. T. Vaniman
K. Wolfsberg
P. O. Box 1663
Los Alamos, NM 87545

Lawrence Berkeley Laboratory (3)
Attn: F. Hale
S. L. Phillips
H. Nitsche
University of California
Berkeley, CA 94720

Martin Marietta Energy Systems, Inc.
Attn: C. S. Fore
Ecological Sciences Information Center
Oak Ridge National Laboratory - Bldg. 2001
P. O. Box X
Oak Ridge, TN 37830

Oak Ridge National Laboratory (4)
Attn: J. A. Carter
G. Jacobs
G. H. Jenks
R. Meyer
Box 2009
Oak Ridge, TN 37831

RE/SPEC, Inc.
Attn: W. Coons
P. F. Gnirk
P.O. Box 14984
Albuquerque NM 87191

RE/SPEC, Inc. (7)
Attn: L. L. Van Sambeek
G. Callahan
T. Pfeifle
J. L. Ratigan
P. O. Box 725
Rapid City, SD 57709

Center for Nuclear Waste Regulatory Analysis (6)
Attn: J. L. Russell (3)
W. Murphy
R. Pabalan
Library
Southwest Research Institute
6220 Culebra Road
San Antonio, TX 78228-0510

Environmental Engineering and Science (2)
Attn: J. O. Leckie
S. W. Park
Department of Civil Engineering
Stanford University
Stanford, CA 94305

Science Applications
International Corporation
Attn: Howard R. Pratt,
Senior Vice President
10260 Campus Point Drive
San Diego, CA 92121

Science Applications
International Corporation
Attn: Michael B. Gross
Ass't. Vice President
Suite 1250
160 Spear Street
San Francisco, CA 94105

Serata Geomechanics
Attn: Dr. Shosei Serata
4124 Lackside Drive
Richmond, CA 94806-1941

Systems, Science, and Software (2)
Attn: E. Peterson
P. Lagus
Box 1620
La Jolla, CA 92038

Westinghouse Electric Corporation (7)
Attn: Library
Lamar Trego
W. P. Poirer
W. R. Chiquelin
V. F.Likar
D. J. Moak
R. F. Kehrman
P. O. Box 2078
Carlsbad, NM 88221

Weston Corporation (1)
Attn: David Lechel
Suite 1000
5301 Central Avenue, NE
Albuquerque, NM 87108

UNIVERSITIES

Arizona State University
Attn: L. P. Knauth
Department of Geology
Tempe, AZ 85287-1404

University of Arizona
Attn: J. G. McCray
Department of Nuclear Engineering
Tucson, AZ 85721

Cornell University
Department of Physics
Attn: Dr. R. O. Pohl
Clark Hall
Ithaca, NY 14853

Florida State University (2)
Attn: J. B. Cowart
J. K. Osmond
Department of Geology
Tallahassee, FL 32308

University of Minnesota
Department of Energy and Materials Science
Attn: R. Oriani
151 Amundson Hall
421 Washington Ave SE
Minneapolis, MN 55455

University of New Mexico (3)
Geology Department
Attn: D. G. Brookins
C. J. Yapp
Library
Albuquerque, NM 87131

New Mexico Institute of Mining and Technology (3)
Attn: L. Brandvold
G. W. Gross
F. Phillips
Socorro, NM 87801

Pennsylvania State University
Materials Research Laboratory
Attn: Della Roy
University Park, PA 16802

Princeton University
Department of Civil Engineering
Attn: George Pinder
Princeton, NJ 08540

Texas A&M University
Center of Tectonophysics
College Station, TX 77840

University of Texas at Austin
Attn: Edward C. Bingler
Deputy Director
Texas Bureau of Economic Geology
Austin, TX 78712

Environmental Engineering and Science (2)
Attn: J. O. Leckie
S. W. Park
Department of Civil Engineering
Stanford University
Stanford, CA 94305

INDIVIDUALS

G. O. Bachman
4008 Hannett Avenue NE
Albuquerque, NM 87110

Carol A. Hill
Box 5444A
Route 5
Albuquerque, NM 87123

Harry Legrand
331 Yadkin Drive
Raleigh, NC 27609

Dennis W. Powers
Star Route Box 87
Anthony, TX 79821

Bob E. Watt
1447 45th St.
Los Alamos, NM 87544

LIBRARIES

Thomas Brannigan Library
Attn: Don Dresp, Head Librarian
106 W. Hadley St.
Las Cruces, NM 88001

Hobbs Public Library
Attn: Ms. Marcia Lewis, Librarian
509 N. Ship Street
Hobbs, NM 88248

New Mexico State Library
Attn: Ms. Ingrid Vollenhofer
P.O. Box 1629
Santa Fe, NM 87503

New Mexico Tech
Martin Speere Memorial Library
Campus Street
Socorro, NM 87810

Pannell Library
Attn: Ms. Ruth Hill
New Mexico Junior College
Lovington Highway
Hobbs, NM 88240

WIPP Public Reading Room
Attn: Director
Carlsbad Public Library
101 S. Halagueno St.
Carlsbad, NM 88220

Government Publications Department
General Library
University of New Mexico
Albuquerque, NM 87131

WIPP PEER PANEL

G. Ross Heath, Chairman
College of Ocean & Fishery Sciences
University of Washington
Seattle, WA 98185

Robert J. Budnitz
President, Future Resources Associates, Inc.
Suite 418
2000 Center Street
Berkeley, CA 94704

Thomas A. Cotton
4429 Butterworth Place NW
Washington, DC 20016

Patrick A. Domenico
Geology Department
Texas A&M
College Station, TX 77843-3115

Charles D. Hollister
Dean for Studies
Woods Hole Oceanographic Institute
Woods Hole, MA 02543

Thomas H. Pigford
Department of Nuclear Engineering
4153 Etcheverry Hall
University of California
Berkeley, CA 94270

Benjamin Ross
Disposal Safety Incorporated
Suite 600
1629 K Street NW
Washington, DC 20006

John Mann
Department of Geology
245 Natural History Building
1301 West Green Street
University of Illinois
Urbana, IL 61801

THE SECRETARY'S BLUE RIBBON PANEL ON WIPP

Dr. Thomas Bahr
New Mexico Water Resources Institute
New Mexico State University
Box 3167
Las Cruces, NM 88003-3167

Mr. Leonard Slosky
Slosky and Associates
Suite 1400
Bank Western Tower
1675 Tower
Denver, Colorado 80202

Mr. Newal Squyres
Eberle and Berlin
P. O. Box 1368
Boise, Idaho 83701

Dr. Arthur Kubo
Vice President
BDM International, Inc.
7915 Jones Branch Drive
McLean, VA 22102

Mr. Robert Bishop
Nuclear Management Resources Council
Suite 300
1776 I Street, NW
Washington, DC 20006-2496

NATIONAL ACADEMY OF SCIENCES, WIPP PANEL

Dr. Charles Fairhurst, Chairman
Department of Civil and
  Mineral Engineering
University of Minnesota
500 Pillsbury Dr. SE
Minneapolis, MN 55455

Dr. John O. Blomeke
Route 3
Sandy Shore Drive
Lenoir City, TN 37771

Dr. John D. Bredehoeft
Western Region Hydrologist
Water Resources Division
U.S. Geological Survey (M/S 439)
345 Middlefield Road
Menlo Park, CA 94025

Dr. Karl P. Cohen
928 N. California Avenue
Palo Alto, CA 94303

Dr. Fred M. Ernsberger
250 Old Mill Road
Pittsburgh, PA 15238

Dr. Rodney C. Ewing
Department of Geology
University of New Mexico
200 Yale, NE
Albuquerque, NM 87131

B. John Garrick
Pickard, Lowe & Garrick, Inc.
2260 University Drive
Newport Beach, CA 92660

John W. Healy
51 Grand Canyon Drive
Los Alamos, NM 87544

Leonard F. Konikow
U.S. Geological Survey
431 National Center
Reston, VA 22092

Jeremiah O'Driscoll
505 Valley Hill Drive
Atlanta, GA 30350

Dr. D'Arcy A. Shock
233 Virginia
Ponca City, OK 74601

Dr. Christopher G. Whipple
Electric Power Research Institute
3412 Hillview Avenue
Palo Alto, CA 94303

Dr. Peter B. Myers, Staff
Director
National Academy of Sciences
Committee on Radioactive
Waste Management
2101 Constitution Avenue
Washington, DC 20418

Dr. Geraldine Grube
Board on Radioactive
Waste Management
GF462
2101 Constitution Avenue
Washington, DC 20418

Dr. Ina Alterman
Board on Radioactive Waste
Management
GF462
2101 Constitution Avenue
Washington, DC 20418

FOREIGN ADDRESSES

Studiecentrum Voor Kernenergie
Centre D'Energie Nucleaire
Attn: Mr. A. Bonne
SCK/CEN
Boeretang 200
B-2400 Mol
BELGIUM

Atomic Energy of Canada, Ltd. (2)
Whiteshell Research Estab.
Attn: Peter Haywood
John Tait
Pinewa, Manitoba, CANADA
R0E 1L0

Dr. D. K. Mukerjee
Ontario Hydro Research Lab
800 Kipling Avenue
Toronto, Ontario, CANADA
M8Z 5S4

Department of Earth Sciences and
Quaternary Sciences Institute
Attn: T. W. D. Edwards
University of Waterloo
Waterloo, Ontario
CANADA N2L 3Gl

Mr. Francois Chenevier, Director (2)
ANDRA
Route du Panorama Robert Schumann
B.P.38
92266 Fontenay-aux-Roses Cedex
FRANCE

Mr. Jean-Pierre Olivier
OECD Nuclear Energy Agency
Division of Radiation Protection
and Waste Management
38, Boulevard Suchet
75016 Paris, FRANCE

Claude Sombret
Centre D'Etudes Nucleaires
De La Vallee Rhone
CEN/VALRHO
S.D.H.A. BP 171
30205 Bagnols-Sur-Ceze
FRANCE

Bundesministerium fur Forschung und
Technologie
Postfach 200 706
5300 Bonn 2
FEDERAL REPUBLIC OF GERMANY

Bundesanstalt fur Geowissenschaften
und Rohstoffe
Attn: Michael Langer
Postfach 510 153
3000 Hannover 51
FEDERAL REPUBLIC OF GERMANY

Hahn-Meitner-Institut fur Kernforschung
Attn: Werner Lutze
Glienicker Strasse 100
100 Berlin 39
FEDERAL REPUBLIC OF GERMANY

Institut fur Tieflagerung (4)
Attn: K. Kuhn
Theodor-Heuss-Strasse 4
D-3300 Braunschweig
FEDERAL REPUPLIC OF GERMANY

Kernforschug Karlsruhe
Attn: K. D. Closs
Postfach 3640
7500 Karlsruhe
FEDERAL REPUBLIC OF GERMANY

Physikalisch-Technische Bundesanstalt
Attn: Peter Brenneke
Postfach 33 45
D-3300 Braunschweig
FEDERAL REPUBLIC OF GERMANY

Hermann Gies
Institut fur Tieflagerung, Gruppe Geochemie
Gesellschaft fur Strahlen und Umweltforschung mbH
Theodor-Heuss-Strasse 4
D-3300 Braunschweig
FEDERAL REPUBLIC OF GERMANY

British Geological Survey (3)
Hydrogeology Group
Attn: G. Darling
R. A. Downing
R. L. F. Kay
Maclean Building
Crowmarsh Gifford
Wallingford
Oxfordshire OX10 8BB
GREAT BRITAIN

U. K. Atomic Energy Authority (3)
Attn: M. Ivanovich
R. Otlet
A. J. Walker
Centre for Nuclear Applications
Isotope Measurement Laboratory
Harwell
Oxfordshire OX11 ORA
GREAT BRITAIN

D. R. Knowles
British Nuclear Fuels, plc
Risley, Warrington, Cheshire WA3 6AS
1002607 GREAT BRITAIN

Shingo Tashiro
Japan Atomic Energy Research Institute
Tokai-Mura, Ibaraki-Ken
319-11 JAPAN

Netherlands Energy Research Foundation
ECN (2)
Attn: Tuen Deboer, Mgr.
L. H. Vons
3 Westerduinweg
P.O. Box 1
1755 ZG Petten, THE NETHERLANDS

Svensk Karnbransleforsorjning AB
Attn: Fred Karlsson
Project KBS
Karnbranslesakerhet
Box 5864
10248 Stockholm, SWEDEN

SANDIA INTERNAL

400	L. D. Tyler
1510	J. C. Cummings
1512	K. L. Erickson
1520	C. W. Peterson
1521	J. G. Arguello
1521	H. S. Morgan
3141	S. A. Landenberger (5)
3151	Supervisor (3)
3154-1	C. L. Ward, (10) for DOE/OSTI
6000	V. L. Dugan, Acting
6230	R. K. Traeger
6232	W. R. Wawersik
6233	D. J. Borns
6233	J. C. Eichelberger
6233	J. L. Krumhansl
6233	S. J. Lambert
6233	C. L. Stein
6300	T. O. Hunter, Acting
6310	T. E. Blejwas, Acting
6313	L. E. Shephard
6315	F. B. Nimick, Acting
6315	R. J. Glass
6315	M. D. Siegel (5)
6340	W. D. Weart
6340A	A. R. Lappin
6340	S. Y. Pickering
6341	R. C. Lincoln
6341	Staff (9)
6341	Sandia WIPP Central Files (10)

6342	D. R. Anderson
6342	Staff (11)
6343	T. M. Schultheis
6343	Staff (2)
6344	E. Gorham
6344	Staff (10)
6345	B. M. Butcher, Acting
6345	Staff (9)
6346	J. R. Tillerson
6346	Staff (7)
8524	J. A. Wackerly (SNLL Library)
9300	J. E. Powell
9310	J. D. Plimpton
9320	M. J. Navratil
9325	L. J. Keck (2)
9330	J. D. Kennedy
9333	O. Burchett
9333	J. W. Mercer
9334	P. D. Seward

*U.S. GOVERNMENT PRINTING OFFICE 1991-0-573-038/44033